6. Observations of Soft and Hard X-Ray Excess Emission in Clusters

Proceedings of the Workshop: *"Diffuse Thermal and Relativistic Plasma in Galaxy Clusters"*
Ringberg Castle, Germany, April 19–23, 1999, eds. H. Böhringer, L. Feretti & P. Schuecker, MPE Report 271, pp. 185-190

Models for the Relativistic Electron Population and Nonthermal Emission in Clusters of Galaxies

Craig L. Sarazin

Department of Astronomy, University of Virginia, P. O. Box 3818, Charlottesville, VA 22903-0818, U.S.A.

Abstract. Models for the integrated relativistic electron population in clusters of galaxies are presented. The results depend on the history of electron acceleration in the cluster. If there is no present particle acceleration or other sources, then no high energy electrons ($\gamma \gtrsim 300$, $E \gtrsim 150$ MeV) should be present due to inverse Compton (IC) losses. High energy electrons are present if particle acceleration is occurring at present, perhaps as a result of a cluster merger shock. The resulting IC, synchrotron, and gamma-ray emission from these models has been calculated. In the models, extreme ultraviolet (EUV) and very soft X-ray emission are a nearly ubiquitous feature, because this emission comes from IC by electrons with the longest lifetimes in clusters. Diffuse UV and optical emission is also expected in most clusters, but at levels which will be difficult to observe. Hard X-ray tails and diffuse radio synchrotron emission are only expected in clusters with recent or current particle acceleration; for example, this acceleration might be due to intracluster merger shocks. Gamma-ray observations at energies of around 100 MeV should detect both the dominant population of relativistic electrons and the corresponding ions. The predicted fluxes are easily detectable with GLAST.

1. Introduction

There are a number of reasons to think that cosmic ray particles might be particularly abundant within the intracluster medium. First, clusters of galaxies should be very effective traps for cosmic ray ions and electrons. Under reasonable assumptions for the diffusion coefficient, particles with energies of less than $\lesssim 10^6$ GeV have diffusion times which are longer than the Hubble time (Colafrancesco & Blasi 1999). Second, the lifetimes of cosmic ray particles, even the electrons which are responsible for most of the radiative signatures of relativistic particles, can be quite long. The radiation fields (optical/IR and X-ray) and magnetic fields ($B \lesssim 1\,\mu$G) in the ICM are low enough that high energy electrons mainly lose energy by inverse Compton (IC) scattering of Cosmic Microwave Background (CMB) photons (Sarazin & Lieu 1998). Lower energy electrons can lose energy by Coulomb interactions with the plasma; however, at the very low densities ($n_e \lesssim 10^{-3}$ cm^{-3}) in the bulk of the ICM, this is only important for electrons with $\gamma \lesssim 200$. (Here, γ is the Lorentz factor for the electrons, so that their total energy is $\gamma m_e c^2$.) For electrons with $\gamma \gtrsim 200$, the lifetime is set by IC losses and is

$$t_{IC} = \frac{(\gamma - 1) m_e c^2}{\frac{4}{3} \sigma_T c \gamma^2 U_{CMB}} \approx 7.7 \times 10^9 \left(\frac{\gamma}{300} \right)^{-1} \text{yr} \,. \qquad (1)$$

The lifetimes of ions are set by interactions; for protons, this gives $t_{ion} \gtrsim 10^{11} (n_e / 10^{-3}\,\text{cm}^{-3})^{-1}$ yr. Thus, clusters of galaxies can retain low energy electrons ($\gamma \sim 300$) and nearly all cosmic ray ions for a significant fraction of a Hubble time.

Clusters of galaxies are likely to have substantial sources of cosmic rays. Clusters often contain powerful radio galaxies, which may produce and distribute cosmic rays throughout the cluster, in addition to possible contributions from the cluster galaxies. However, the primary reason why the cosmic ray populations in clusters might be large is connected with the high temperature of the intracluster gas. This indicates that all of the intracluster medium (typically, $10^{14}\,M_\odot$ of gas) has passed through strong shocks with shock velocities of $\sim$1000 km/s during its history. In our own Galaxy, whenever diffuse gas undergoes a strong shock at velocities of this order, a portion of the shock energy goes into the acceleration of relativistic particles (e.g., Blandford & Eichler 1987) Thus, it seems likely that relatively efficient particle acceleration also occurs in clusters of galaxies.

Direct evidence for the presence of an extensive population of relativistic particles and magnetic fields in the ICM comes from the observation of diffuse synchrotron radio halos in clusters (e.g., Giovannini et al. 1993). More recently, extreme ultraviolet (EUV) and very soft X-ray emission has been detected from a number of clusters (Lieu et al. 1996a,b; Mittaz, Lieu, & Lockman 1998). One hypothesis is that this radiation is inverse Compton (IC) emission by relativistic electrons (Hwang 1997; Enßlin & Biermann 1998; Sarazin & Lieu 1998). Finally, hard X-ray emission has recently been detected in clus-

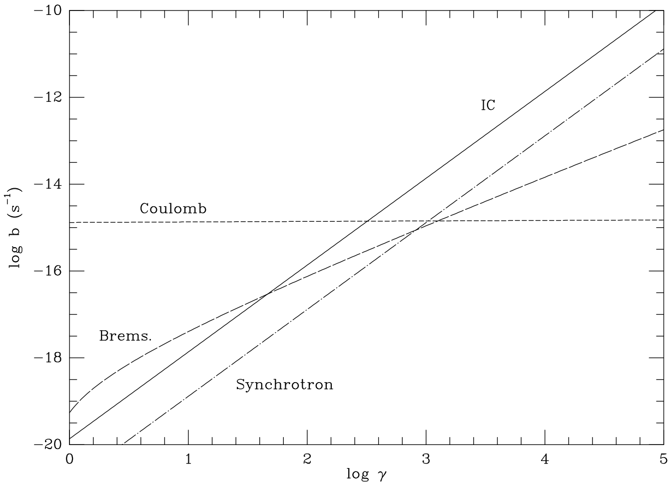

Fig. 1. The values of the losses function $b(\gamma)$ for inverse Compton (IC) emission, Coulomb losses, synchrotron losses, and bremsstrahlung losses as a function of γ. The values assume $n_e = 10^{-3}$ cm^{-3}, $B = 1\,\mu$G, and $z = 0$.

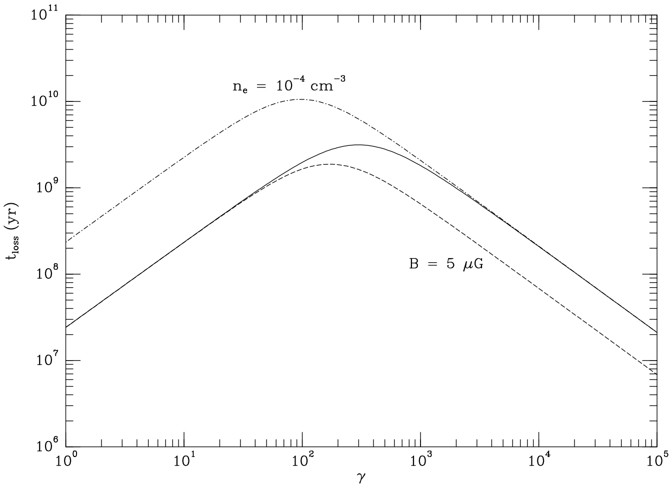

Fig. 2. The solid curve gives the loss time scale t_{loss} as a function of γ for electrons in a cluster with an electron density of $n_e = 10^{-3}$ cm^{-3} and a magnetic field of $B = 1$ μG. The short-dash curve is for $B = 5$ μG, while the dash-dot curve is for $n_e = 10^{-4}$ cm^{-3}.

ters with *BeppoSAX*, which might be due to IC emission from higher energy electrons (Fusco-Femiano et al. 1999; Kaastra, Bleeker, & Mewe 1998). The EUV emission would require electrons with $\gamma \sim 300$, while the hard X-ray emission would require $\gamma \sim 10^4$.

In this paper, illustrative models will be presented for the integrated energy spectrum of primary, relativistic electrons, under the assumption that they remain trapped in the cluster (Colafrancesco & Blasi 1999). More details on these models are given in Sarazin (1999). Radio synchrotron and inverse Compton emission spectra will be determined up to the hard X-ray spectral band. Gamma-ray emission by the same electrons (as well as emission by ions through π^o decay) will also be discussed briefly.

2. The Electron Spectrum in Clusters

I will use the Lorentz factor γ of the electrons as the independent variable rather than the kinetic energy $E = (\gamma - 1)m_e c^2$, where m_e is the electron mass. Let $N(\gamma)d\gamma$ be the total number of electrons in the cluster with energies in the range γ to $\gamma + d\gamma$, and let $Q(\gamma)d\gamma$ be the total rate of production of new cosmic ray this energy range. The equation for the electron spectrum is then

$$\frac{\partial N(\gamma)}{\partial t} = \frac{\partial}{\partial \gamma}\left[b(\gamma)N(\gamma)\right] + Q(\gamma)\,, \tag{2}$$

where $b(\gamma) = -d\gamma/dt$ gives the energy loss by an individual electron.

The loss function includes IC emission, Coulomb losses, synchrotron losses, and bremsstrahlung losses. In Fig. 1, these loss rates are shown as a function of γ for typical cluster conditions. IC losses dominate at high energies $\gamma \gtrsim 200$, while Coulomb losses dominate at low energies. Values for the loss time scale, defined as $t_{loss} \equiv \gamma/b(\gamma)$, are shown in Fig. 2. The lifetime is maximum at $\gamma \approx 300$, where they are $\sim 3 - 10$ Gyr, which is comparable to the likely ages of clusters.

The nature of the resulting electron populations depends on whether there is a current or very recent ($z \lesssim 0.03$) source of particles in the clusters, such as an ongoing merger shock, or the electrons were all accelerated in the past ($0.03 \lesssim z \lesssim 1$). In all of the models shown here, the accelerated electrons have a power-law spectrum, $Q(\gamma) = Q_1\gamma^{-p}$ with $p = 2.3$, and the electron spectra are normalized such that the total kinetic energy injected in electrons with $\gamma \geq 300$ is $E^{tot}_{CR,e} = 10^{63}$ ergs. Fig. 3 shows the present-day electron spectra in a series of models without any current source of newly accelerated particles. Thus, these models might apply to a cluster which is not currently undergoing a subcluster merger. At low energies, the electron population is reduced and the shape flattened by Coulomb losses. At high energies, the electron population is reduced and the shape of the spectrum steepened by IC and synchrotron losses. Because the IC and synchrotron losses increase with the square of the electron energy, there is an upper cut-off to the electron distribution; no electrons are found at energies higher than γ_{max}. Because the energy density in the CMB increases as $(1+z)^4$, the IC losses increase rapidly at high redshift. If there is no electron acceleration since $z \gtrsim 1$, the value of $\gamma_{max} \lesssim 100$, and Coulomb losses remove all of the lower energy electrons. In order to have any significant population of primary electrons with $\gamma \gtrsim 10^2$ at the present time, there must have been a substantial injection of particles into clusters at moderately low redshifts, $z \lesssim 1$.

Fig. 4 shows the resulting present-day electron spectra in models in which there is a current source of accelerated electrons, such as a cluster merger shock. Again, Coulomb losses reduce and flatten the electron population at low en-

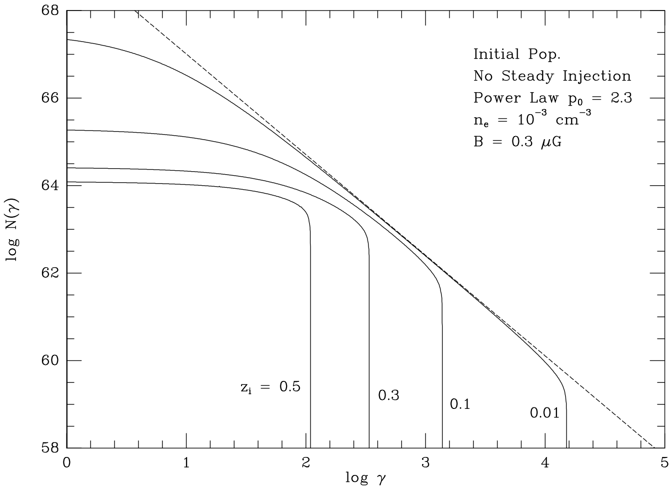

Fig. 3. The present day relativistic electron populations in models with no current particle acceleration (e.g., no subcluster merger at present). An initial population of electrons, which is shown as a dashed line, was introduced into the cluster at a redshift of $z_i = 0.01$, 0.1, 0.3, and 0.5.

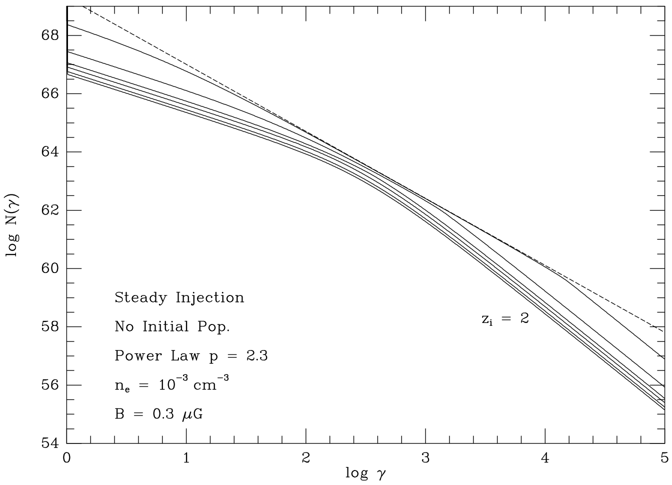

Fig. 4. The present day relativistic electron populations in a series of models with ongoing particle acceleration, perhaps due to a cluster merger shock. he solid curves show models for clusters which started at redshifts of $z_i = 2$, 1, 0.5, 0.3, 0.1, and 0.01 (bottom to top). The short-dashed curve gives the total power-law spectrum of all of the injected particle over the cluster lifetime.

ergies, and IC and synchrotron losses reduce and steepen the electron population at high energies. However, these losses don't remove the high energy particles completely, as new particles are always being accelerated. Instead, the population quickly relaxes into steady-state, where the low (high) energy population is one power flatter (steeper) than the injected electrons (Ginzburg & Syrovatskii 1964).

Finally, we consider models in which there is an initial population in the cluster, and in which there also is current injection of new particles. These might apply to the more realistic cases where the cluster had particle acceleration associated with the formation of the cluster and mergers in the past, but also has a subcluster merger occurring at present. An illustrative set of such models are shown in Fig. 5. The different models are characterized by differing values of F_{inj}, which is the fraction of the particle energy which has been injected by the current steady injection process, as opposed to the earlier population. If the electrons were injected in cluster shocks, then F_{inj} might be roughly proportional to the fraction of the thermal energy content of the ICM which is being generated in the current shock. The general features of these models are that the electron spectrum is moderately flat below $\gamma \approx 300$. Unless there is a very strong present merger or other current particle source, the electron population drops off rapidly above $\gamma \approx 300$. In most models for clusters, most of the relativistic electron energy should be in particles with $\gamma \approx 300$; these are the particles with the longest lifetimes (Fig. 2). If a cluster has a ongoing merger or other particle source, then there will also be a high energy tail to the particle distribution. Because this tail is likely to be in steady-state, the electron distribution is likely to be one power steeper than the source, perhaps $N(\gamma) \propto \gamma^{-3.3}$.

3. Inverse Compton Emission

The emission produced by the relativistic electron populations through the inverse Compton scattering of CMB photons was also calculated. Let $L_\nu d\nu$ be the luminosity of IC emission at frequencies from ν to $\nu + d\nu$. Then, the spectrum of IC emission is related to the electron spectrum $N(\gamma)$ by

$$L_\nu = 12\pi\sigma_T \int_1^\infty N(\gamma)\, d\gamma \int_0^1 J\left(\frac{\nu}{4\gamma^2 x}\right) \mathcal{F}(x)\, dx\,, \quad (3)$$

where $\mathcal{F}(x) \equiv 1 + x + 2x \ln x - 2x^2$. Here, $J(\nu)$ is the mean intensity at a frequency ν of the radiation field being scattered. For the CMB, this is just the black body function $J(\nu) = B_\nu(T_{CMB})$. For a power-law electron spectrum $N(\gamma) \propto \gamma^{-p}$, the IC spectrum is a power-law $L_\nu \propto \nu^\alpha$, where $\alpha = -(p-1)/2$. This gives $\alpha = -0.65$ for the injection spectrum of $p = 2.3$.

Fig. 6 shows the resulting IC spectra for a variety of different models; for details of the specific models, see Sarazin (1999). Model 1 has a current source of electrons; for example, this might be due to a subcluster merger. At frequencies above 10^{17} Hz, the spectrum quickly steepens with time due to IC losses, and becomes a half power steeper than that given by the injected electron spectrum, $\alpha \approx -(p/2) \approx -1.15$. At low frequencies, the spectrum flattens more gradually due to Coulomb losses, approaching a spectrum which is a half power flatter than that due to the injected spectrum, $\alpha \approx -(p-2)/2 \approx -0.15$. If the current acceleration process has occurred since a redshift of $z \gtrsim 0.2$, the spectrum is near that of a steady-state electron population, with these two power-laws meeting

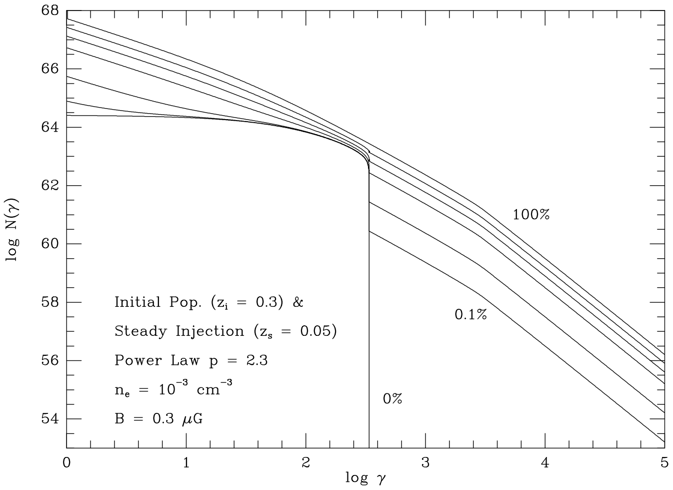

Fig. 5. The electron energy spectra in models with both an initial electron population and current injection of new particles, perhaps due to an ongoing cluster merger. The values of the fraction of particle energy due to current injection are (top to bottom) $F_{inj} = 100\%$, 50%, 25%, 10%, 1%, 0.1%, and 0%.

at a knee at $\nu \sim 3 \times 10^{16}$ Hz. If the current acceleration process is more recent, there is a central region of the IC spectrum where the electrons are not yet in steady-state. Here, the spectral index is $\alpha \approx -0.65$.

Models 11 and 22 have no current source of electrons (e.g., no ongoing cluster merger). The electron energy distributions of these models have a cut off at high energies, γ_{max}, which results from rapid IC and synchrotron losses by high energy electrons (see Fig. 3). As a result, the IC spectra have a very rapid fall off at high energies (exponentially or slightly faster; see eq. [54] in Sarazin [1999]).

At low frequencies, the IC spectra of models without current acceleration flatten and become slowly increasing with frequency as the models age. We expect that the low energy electron spectrum in an older model without current acceleration will become nearly independent of γ except for a slowly varying logarithmic factor (see eq. 36 in Sarazin [1999]). If $N(\gamma) \approx N_{low}$ = constant at low energies, then the low frequency IC spectrum varies as $L_\nu \propto \nu^{1/2}$.

Model 27 in Fig. 6 shows the spectrum of a model with both an initial population of particles and electron acceleration at the present time. In this model, the fraction of electrons being contributed by the current acceleration (e.g., current merger shock) is $F_{inj} = 1\%$. Models in which the current rate of particle injection provides a small but significant fraction of the total electron energy have hybrid spectra. At low frequencies ($\nu \lesssim 10^{17}$ Hz), they have an extended hump of emission, with a rapid fall off above $\nu \sim 10^{16}$ Hz. However, they also have an extended hard tail of emission at high frequencies, which has a power-law spectrum with a spectral index of $\alpha \approx -(p/2) \approx -1.15$. At the bottom of Fig. 6, there is a scale which shows the portion of the electromagnetic spectrum involved.

3.1. EUV and Soft X-ray Emission

Fig. 6 shows that the fluxes from different models all tend to agree at frequencies $\sim 2 \times 10^{16}$ Hz, which corresponds to a photon energy of ~80 eV. Thus, EUV and very soft X-ray emission might be expected to be a universal property of clusters of galaxies, if they have all produced populations of relativistic electrons with total energies which are at least $\sim 10^{-2}$ of their thermal energies. The one constraint is that at least a portion of these particles must have been injected at moderate to low redshifts, $z \lesssim 1$. The fact that essentially all of the models produce a strong and similar flux at EUV energies may help to explain the fact the excess EUV emission has been detected in all of the cluster observed with the *Extreme Ultraviolet Explorer* (*EUVE*) satellite and which lie in directions of sufficiently low Galactic columns that this radiation is observable (Lieu et al. 1996a,b; Mittaz, Lieu, & Lockman 1998; Sarazin & Lieu 1998). Values of $L_\nu(EUV)$ at a frequency of $v = 2 \times 10^{16}$ Hz are listed in Table 3 of Sarazin (1999). From these values, one finds that the emission at EUV energies is fairly directly related to $E_{CR,e}^{tot}$, the total amount of energy injected in electrons with $\gamma \geq 300$. The average relationship is about

$$L_\nu(EUV) \sim 6 \times 10^{27} \left(\frac{E_{CR,e}^{tot}}{10^{63}\,\mathrm{ergs}} \right) \mathrm{ergs}\,. \qquad (4)$$

Models which are likely to apply to real clusters agree with equation (4) to within a factor of 4.

While the amount of EUV emission is fairly constant from model to model, the spectrum depends strongly on the amount of recent particle injection. Very steeply declining spectra occur in models without current particle acceleration and with small values of γ_{max}. For many of the models, the spectra can be fit by a power-law with $-1.5 \gtrsim \alpha_{EUV} \gtrsim -0.6$, but very large negative values also occur. The spectrum drops more rapidly with frequency as the proportion of electrons which are currently being accelerated decreases.

Because the *EUVE* observations of clusters have no spectral resolution, there is no detailed information on the observed spectrum of EUV emission (Lieu et al. 1996a,b; Mittaz, Lieu, & Lockman 1998). However, the ratio of *EUVE* fluxes to those in the softest bands of the *ROSAT* PSPC suggest that the EUV spectra are generally steeply declining. The spectra of the Coma cluster is less steeply declining than that of Abell 1795; this might be understood as the result of particle acceleration by merger shocks, since Coma appears to be undergoing a merger or mergers (e.g., Burns et al. 1994), while Abell 1795 appears regular and relaxed (e.g., Briel & Henry 1996). Also, the EUV spectra appear to get steeper with increasing radius in the Abell 1795 cluster (Mittaz, Lieu, & Lockman 1998). This might be the result of decreasing gas density with radius, which will decrease the effect of Coulomb loses at low energies (Fig. 2).

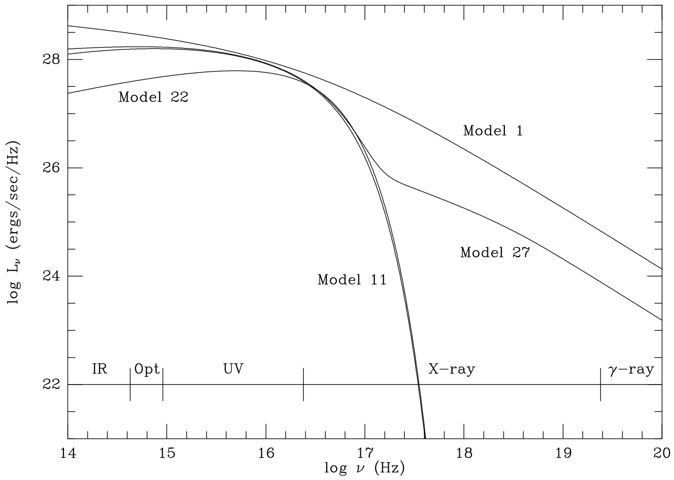

Fig. 6. The IC emission spectra for different types of cluster models (for details on the models, see Sarazin [1999]). Models 1 has current electron acceleration (perhaps due to an ongoing merger shock), but no initial electron population (see Fig. 4). Model 11 has an initial electron population (perhaps due to the formation of the cluster or earlier mergers), but no current electron acceleration (see Fig. 3). Model 22 is identical to Model 11, but the initial electron energy spectrum has a break at an energy of 1 GeV. Model 27 has both an initial electron population, and a source of electrons at present (see Fig. 5). The scale near the bottom of the Figure shows the portion of the electromagnetic spectrum.

3.2. Hard X-ray IC Emission and Radio Halos

At photon energies of 0.5 to 10 keV, the dominant emission in most clusters is the thermal emission from the hot ICM, and IC emission will be difficult to detect. However, at energies $\gtrsim$20 keV, IC emission should again become observable, assuming that it is dropping as power-law function of frequency, while the thermal emission drops as an exponential. IC emission at photon energies of $\sim$50 keV will be produced by electrons with $\gamma \sim 10^4$. These particles have rather short lifetimes ($t_{loss} \ll 10^9$ yr), and are only present in clusters in which there has been substantial electron acceleration since $z \lesssim 0.03$. As Fig. 6 shows, only the models with current or very recent particle acceleration have any significant HXR emission.

Because of the short lifetimes of the particles producing HXR emission, these electrons are likely to be close to steady-state if present in significant quantities. The expected steady-state spectral index if IC losses dominated would be $\alpha_{HXR} = -(p+1)/2 \approx -1.65$. The best-fit spectral indices are flatter than this, $\alpha_{HXR} \approx -1.1$, mainly because other loss processes are important at the lower energy end of the HXR band (Fig. 1). All of the HXR spectral shapes in the models are very similar, as expected for steady-state populations. The differences in the HXR luminosities just reflect differences in the present rate of electron acceleration. To a good approximation, the present day value of the hard X-ray IC luminosity L_{HXR} (20–100 keV) is simply given by

$$L_{HXR} \approx 0.17 \dot{E}_{CR,e}(\gamma > 5000) \, . \qquad (5)$$

where $\dot{E}_{CR,e}(\gamma > 5000)$ is the total present rate of injection of energy in cosmic ray electrons with $\gamma > 5000$. The best-fit coefficient (0.17 in eqn. 5) depends somewhat on the power-law index of the injected electrons; the value of 0.17 applies for $p = 2.3$.

The same relativistic electrons which produce HXR emission by IC scattering will also produce radio emission by synchrotron emission. The synchrotron radio emission from these models is given in Sarazin (1999). Electrons with a Lorentz factor of γ produce radio emission with $\nu \sim 100(B/\mu G)(\gamma/10^4)^2$ MHz, and rather high electron energies ($\gamma \gtrsim 10^4$) are needed to produce observable radio emission. Thus, these are likely to be the same electrons which produce the hardest HXR emission. In general, HXR emission and radio synchrotron emission are expected only in clusters with very recent or current acceleration of relativistic electrons. Thus, both measure the current rate of particle injection. For example, if the particles are accelerated in ICM shocks, HXR and radio emission would be expected only in clusters which are currently undergoing (or which very recently underwent) a merger.

Recently, excess hard X-ray emission has been detected in the Coma (Fusco-Femiano et al. 1999) and Abell 2199 (Kaastra, Bleeker, & Mewe 1998) clusters with *BeppoSAX*. It is tempting to attribute this HXR radiation to IC emission from higher energy electrons. Of course, Coma has a radio halo and abundant evidence for merger activity. Thus, it is consistent with this hypothesis, although the required magnetic field ($B = 0.15$ μG) is smaller than might have been expected. On the other hand, Abell 2199 is a relaxed cluster with a strong cooling flow. It has no radio halo emission, with an upper limit on the radio flux which is inconsistent with the IC interpretation of the HXR emission unless $B \lesssim 0.01$ μG (Kempner & Sarazin 1999). Thus, it seems unlikely that the HXR in Abell 2199 is due to IC scattering of CMB photons. It is possible that part of the HXR emission may be due to nonthermal bremsstrahlung (bremsstrahlung from superthermal but not strongly relativistic electrons).

3.3. Optical and UV Emission

One also expects that the lower energy portion of the cosmic ray population in clusters will produce diffuse optical and UV emission. Diffuse optical emission is known to exist in many clusters, particularly in those with central cD galaxies (e.g., Boughn & Uson 1997). Although the origin is not completely understood, the optical colors of the diffuse light suggest that it is due to old stars, which may have been stripped from cluster galaxies. It is likely that the near or vacuum UV are better regions to detect low surface brightness diffuse emission due to IC emission, since the older stellar population in E and S0 galaxies (and, presumably, the intracluster stellar population) are fainter there.

The IC optical-UV emission from the models is given in Sarazin (1999). The predicted fluxes are rather low when compared to the diffuse optical emission seen in clusters of galaxies or to the sensitivity of current and UV instruments for detecting diffuse emission. The UV powers of most of the models lie within a relatively narrow range of about an order of magnitude. Unless the electron density in the ICM is much higher than 0.001 cm^{-3} and Coulomb losses are catastrophic or the electron population in clusters is very old, one would always expect a significant population of lower energy electrons. The IC spectra in the optical and UV are fairly flat, with spectral indices of $-0.5 \gtrsim \alpha_{Opt,UV} \gtrsim 0.3$. In models with current electron acceleration, the lower energy electron population should be approaching steady-state with the Coulomb losses, and the expected power-law for the IC emission is $\alpha \approx -(p-2)/2 \approx -0.15$. For models without current acceleration, the electron spectrum is expected to be nearly flat at low energies, and the $L_\nu \sim \nu^{1/2}$. Thus, the spectral index should be slightly positive in these models.

4. Gamma-Ray Emission

The same relativistic electrons and ions will produce gamma-ray emission. This involves a wide variety of physical processes; in the interest of brevity, only the region around 100 MeV will be discussed here. The two major emission processes in this region of the gamma-ray spectrum are electron bremsstrahlung (due to collisions between relativistic electrons and thermal ions and electrons), and π^o decay, due to collisions between relativistic ions and thermal ions). Fig. 7 shows the predicted spectrum for the Coma cluster. The electron population was determined by the IC emission required to fit the observed *EUVE* flux and *EUVE/ROSAT* flux ratio (Lieu et al. 1996a). The ratio of the π^o decay component to the bremsstrahlung component is determined by the ratio of relativistic ions to electrons. In Fig. 7, this ratio was taken to be 10.

The predicted flux of gamma-rays with $h\nu \geq 100$ MeV is about 2×10^{-8} $\mathrm{cts/cm^2/s}$. For comparison, the *EGRET* upper limit on the flux from Coma in this range is $\leq 4 \times 10^{-8}$ $\mathrm{cts/cm^2/s}$ (Sreekumar et al. 1996). Thus, it seems certain that *GLAST* will detect Coma and many other clusters, assuming that the detected EUV emission from clusters is due to IC from relativistic electrons. The measurement of the gamma-ray spectrum in the region around 100 MeV will allow the ratio of relativistic ions to electrons to be determined. In many astrophysical environments, this is an unknown quantity. The *EGRET* limit already implies that this ratio is $\lesssim 30$ in the Coma cluster.

Acknowledgements. This work was supported in part by NASA Astrophysical Theory Program grant NAG 5-3057. I would like to thank Hans Böhringer and Luigina Feretti for organizing such an enjoyable and useful workshop.

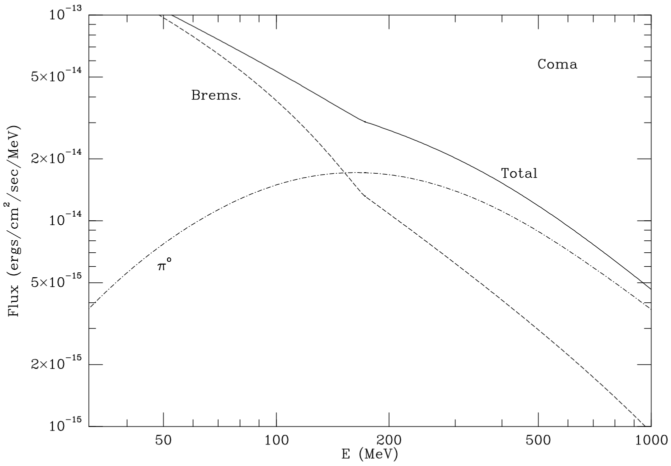

Fig. 7. The predicted gamma-ray spectrum of the Coma cluster in the region around 100 MeV. The emission is mainly the result of bremsstrahlung by relativistic electrons and π^o decay due to relativistic ions. The electron population was determined by the best-fit *EUVE* fluxes and spectra. The ions have 10 times the electron energy.

References

[1] Blandford, R. D., & Eichler, D. 1987, Phys. Rep., 154, 1
[2] Boughn, S. P., & Uson, J. M. 1997, ApJ, 488, 44
[3] Briel, U. G., & Henry, J. P. 1996, ApJ, 472, 131
[4] Burns, J. O., Roettiger, K., Ledlow, M., & Klypin, A. 1994, ApJ, 427, 87
[5] Colafrancesco, S., & Blasi, P. 1998, APh, 9, 227
[6] Enßlin, T. A., & Biermann, P. L. 1998, A&A, 330, 90
[7] Fusco-Femiano, R., et al., 1999, ApJ, 513, L21
[8] Ginzburg, V. L., & Syrovatskii, S. I. 1964, The Origin of Cosmic Rays (New York: MacMillan)
[9] Giovannini, G., Feretti, L., Venturi, T., Kim, K. T., & Kronberg, P. P. 1993, ApJ, 406, 399
[10] Hwang, C.-Y. 1997, Science, 278, 1917
[11] Kaastra, J. S., Bleeker, J. A. M., & Mewe, R. 1998, Nucl. Phys. B, 69, 567
[12] Kempner, J., & Sarazin, C. L. 1999, ApJ, submitted
[13] Lieu, R., Mittaz, J. P. D., Bowyer, S., Breen, J. O., Murphy, E. M., Lockman, F. J., & Hwang, C.-Y. 1996a, Science, 274, 1335
[14] Lieu, R., Mittaz, J. P. D., Bowyer, S., Lockman, F. J., Hwang, C.-Y., & Schmitt, J. H. M. M. 1996b, ApJ, 458, L5
[15] Mittaz, J. P. D., Lieu, R., & Lockman, F. J. 1998, ApJ, 498, L17
[16] Sarazin, C. L. 1999, ApJ, 520, in press
[17] Sarazin, C. L., & Lieu, R. 1998, ApJ, 494, L177
[18] Sreekumar, P., et al., 1996, ApJ, 464, 628

Proceedings of the Workshop: *"Diffuse Thermal and Relativistic Plasma in Galaxy Clusters"*
Ringberg Castle, Germany, April 19–23, 1999, eds. H. Böhringer, L. Feretti & P. Schuecker, MPE Report 271, pp. 191-196

Hard X-Ray Emission in Clusters of Galaxies

Roberto Fusco-Femiano

Istituto di Astrofisica Spaziale/CNR, Area Ricerca di Roma Tor Vergata, via del Fosso del Cavaliere, 00133 Roma, Italy

Abstract. Hard X-ray radiation has been detected for the first time in the Coma cluster by *BeppoSAX* and *RXTE* . *BeppoSAX* observations report also a marginal evidence of a hard tail in the A2199 and A2256 spectra. In particular, I discuss the possible interpretations that have been proposed for the nonthermal emission detected in the Coma cluster up to $\sim$ 80 keV in excess of thermal above $\sim$ 25 keV.

1. Introduction

The study of clusters of galaxies has benefited greatly by extensive X-ray measurements of thermal emission from hot intracluster gas. Spectral and imaging observations of clusters have resulted in direct determinations of the gas temperature, density and abundances, and in reliable estimates of the baryonic and total masses of clusters. The sample of observed X-ray clusters has given us some insight into the cosmological evolution of this class of objects. These important results have been obtained in large part from measurements of X-rays at energies $\leq$ 10 keV.

Only few attempts to detect radiation at energies above $\sim$ 30 keV have been made. The observations with ballon experiments (Bazzano et al. 1984; 1990), with HEAO-1 (Rephaeli, Gruber & Rothschild 1987) and with the OSSE experiment (Rephaeli, Ulmer & Gruber 1994) onboard the *Compton* GRO satellite, reported essentially flux upper limits. Observations of clusters at high X-ray energies (HEX) are of considerable interest considering that we can derive significant additional information on physical conditions in the intracluster environment, due to the very different emission mechanism. This emission was predicted in clusters showing radio halos that assure the presence of relativistic electrons in the intracluster space of about ten clusters. The emission mechanism is due to inverse Compton scattering of relativistic electrons by the cosmic microwave background (CMB) radiation. Recently, different models have been proposed that will be discussed in section 3.

The much improved spectral capabilities of *BeppoSAX* and *RXTE* satellites have recently led to a significant breakthrough in the measurement of this additional spectral component in clusters. Hard X-ray radiation has been detected in the Coma cluster up to $\sim$ 80 keV (Fusco-Femiano et al. 1999; Rephaeli, Gruber & Blanco 1999) while a marginal evidence is present in the A2199 (Kaastra et al. 1999) and A2256 (Fusco-Femiano et al. , in preparation) spectra.
Could these hard tails be detected by previous missions ?

The imaging spectroscopy missions either did not have sufficient bandpass (*Einstein* IPC, *ROSAT* PSPC), or too low sensitivity (or often too short exposure) (*ASCA*). Other missions had no imaging capabilities in the 2-10 keV band (*Ginga*) or had too low sensitivity above 10 keV. It is the wide bandpass combined with the low-background orbit and the high sensitivity of *BeppoSAX* that allow these hard tails to be detected for the first time. In particular, we exploited the unique capabilities of the PDS : a) the minimum detectable source intensity in the 30-80 keV range is $\sim 2 \times 10^{-6}$ $ph/cm^2\ s\ keV$) ; b) a small Field of View (FOV), 1.3° hexagonal, to reduce source confusion; c) a low and stable background thanks to the equatorial orbit of *BeppoSAX* . Another important feature is the wide energy coverage in order to independently measure the tail of the thermal emission.

2. Hard X-ray Emission from the Coma Cluster

The Coma cluster was observed by *BeppoSAX* in December 97 for $\sim$ 91ksec. We started the spectral analysis by working only with the PDS data to have a robust indication of the presence of a non-thermal component in the observed HXR radiation. The MECS data are not very helpful in this respect, as its field of view is much smaller than that of the PDS. However, with the PDS data alone, it is not possible to perform complex spectral fits, so we need to fix the temperature of the intracluster medium that it is in the range of 7.5-8.5 keV, as measured by several observatories (Hughes et al. 1988; Hughes, Gorenstein & Fabricant 1988; Watt et al. 1992; Hughes et al. 1993). The average cluster temperature depends on the FOV of the instrument: the larger the field of view the lower is the measured temperature. This reflects the presence of a temperature

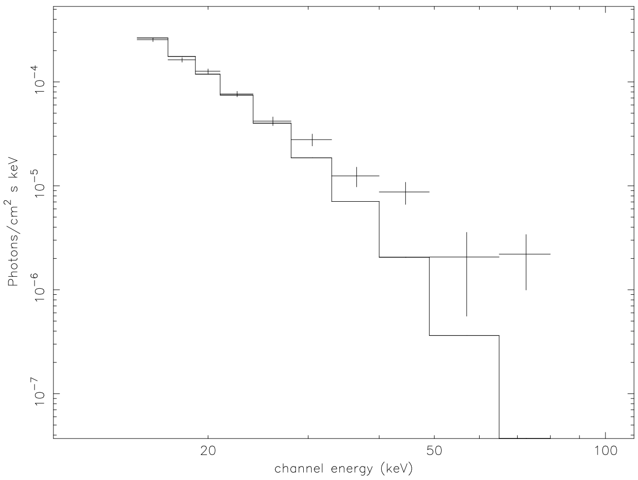

Fig. 1. PDS data. The continuous line represents the best fit with a thermal component at the average cluster gas temperature of 8.21 keV (Hughes et al. 1993).

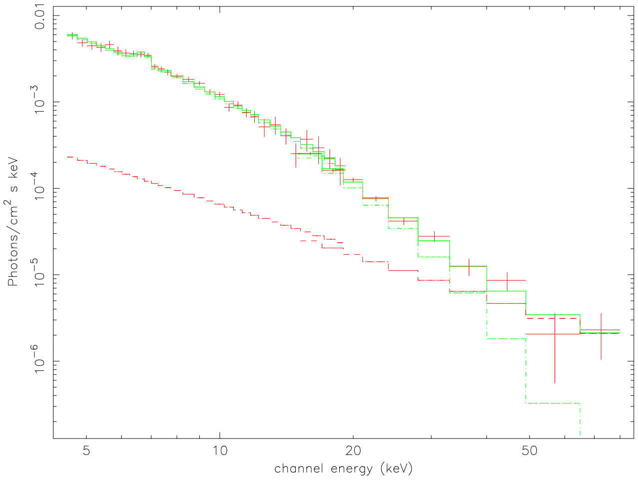

Fig. 2. The continuous line is the best-fit to the HPGSPC (4.5-20 keV) and PDS data (15-80 keV). The dashed line represents the thermal component (kT=$8.5^{+0.6}_{-0.5}$ keV), while the dashed straight line is the non-thermal component with a spectral index of 1.6. A constant value of 0.90 takes into account the relative calibration of the two data sets. The χ^2_{red} is 0.80 for 34 d.o.f..

gradient in the intracluster gas of Coma. We adopted cluster value of 8.21 keV, as determined by the Large Area Counter (LAC) experiment onboard *Ginga* (whose field of view of $1^\circ \times 2^\circ$ is not much different from that of the PDS). Hovever, also adopting a temperature as high as 9.1 keV, as observed by the MECS in the cluster core, the results are substantially the same. We performed spatially resolved spectroscopy within a region 8 arcmin in radius with concentric annuli of 2 arcmin (the results will be discussed in detail in a forthcoming paper). So, the continuous line in Fig. 1 is a thermal component at the average cluster gas temperature of 8.2 keV.

There is a clear excess above 25 keV at a 4.5 σ level. Fitting with a single thermal component, we obtain a value of kT=$10.73^{+0.81}_{-0.74}$ keV and the reduced χ^2 is 2.14 for 8 degrees of freedom. The χ^2 value has a significant decrement when a second component is added. Modelling this second component as a power law, as for non-thermal emission, the reduced χ^2 value is 0.92 for 7 degrees of freedom. The confidence interval for the power law spectral index is rather large, 0.7-3.6, but the flux ($\sim 2.2 \times 10^{-11}$ erg/cm^2 s in the 20-80 keV energy range), is rather stable against variations of the photon spectral index. On the other hand, if we consider a second thermal component, instead of the non-thermal one, the fit requires a temperature greater than 40 keV. This unrealistic value may be interpreted as a strong indication that the detected hard excess is due to a non-thermal mechanism.

A tighter constraint on the photon spectral index can be obtained considering also the HPGSPC data in the 4.5-20 keV energy range, that has a field of view ($1^\circ \times 1^\circ$) comparable to that of the PDS, and therefore can be used for a global spectral fit.

Combining HPGSPC and PDS data it is then possible to leave the temperature of the intracluster medium as a free parameter in the fit procedure. We obtain an ICM temperature of $8.5^{+0.6}_{-0.5}$ keV, consistent with the *Ginga* determination, and an iron abundance of $0.15^{+0.6}_{-0.4}$. The reduced χ^2 is 0.80 for 34 degrees of freedom. The spectral index range is 0.7-2.5, smaller than the previous one determined using only the PDS data, but still not sufficient to distinguish between different emission mechanisms. If we fix the parameters of the thermal component to their best-fit values we obtain $1.57^{+0.36}_{-0.39}$ (90%) for the photon index of the non-thermal radiation, corresponding to a contribution of the non-thermal emission to the flux in the range 2-10 keV between $\sim (2-10)\%$.

3. Possible Interpretations of the Hard X-ray Excess

In this section, I will discuss the possible interpretations that have been proposed to explain the nonthermal radiation detected by the PDS in the energy spectrum of the Coma cluster.

3.1. Different Source in the Field of View of the PDS

One possible explanation for the observed excess is emission by a different source in the field of view of the PDS. The most qualified candidate is the Seyfert 1 galaxy X Comae (z=0.092±0.002; Bond & Sargent 1973) that has been observed by *ROSAT* PSPC (Dow & White 1995) that reports a power law spectrum with photon index 2.50±0.16 and a flux of 3.6×10^{-12} erg/cm^2 s in the 0.4-2.4 keV band

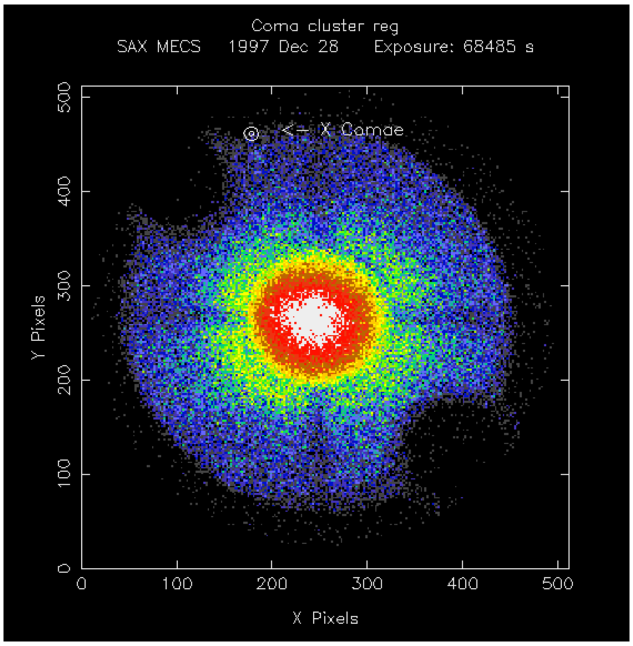

Fig. 3. The X-ray image of the Coma cluster by MECS; the location of the source X Comae is reported.

(corresponding to $\sim 1.6 \times 10^{-12}$ erg/cm^2 s in the range 2-10 keV). X Comae has been observed also by *EXOSAT* (Branduardi-Raymont et al. 1985) and by *Einstein* IPC Slew Survey (Elvis et al. 1992) at approximately the same flux level. The steep photon index reported by *ROSAT* requires an unusual variability of a factor ~65 to explain the detected hard excess, considering that the source is $\sim 27'$ off-axis and $N_{\rm H,gal} = 9 \times 10^{19}$ cm^{-2}. With a more typical photon index of 1.8 the variability factor is ~11, that is still large, but not uncommon. Luckily enough, X Comae is located just on the edge of the field of view of the MECS, and part of the Point Spread Function (PSF) of the source lies within the field of view of the detector (see Fig. 3). Considering the location of X Comae and the lack of detection, it is possible to estimate an upper limit to the flux of the source of the order of $\sim 4 \times 10^{-12}$ erg/cm^2 s (2-10 keV), much lower than the flux of $\sim 2.9 \times 10^{-11}$ erg/cm^2 s (photon index = 1.8) required to account for the HXR. So, it is very unlikely that the hard excess detected by the PDS may be due to X Comae.

We have the possibility to investigate the presence of point sources also in the outermost regions of the cluster using the 14 pointings of *ASCA* that cover the region observed by the FOV of the PDS. This check is necessary in order to verify the presence of sources like Circinus, an obscured Seyfert 2 galaxy, that shows a very large column density of $\sim 10^{24}$ cm^{-2} and it is very active above 10 keV (Matt et al. 1999). This research is actually in progress. The probability to find this kind of sources in the 2 square degree of the PDS is $\sim (8-10)\%$; Fusco-Femiano et al. , in preparation).

3.2. Inverse Compton Model

Assuming that the hard spectral tail is due to relativistic electrons scattering the CMB photons, it is possible to derive, using only observables, the value of the mean volume-averaged intracluster magnetic field, B, of the intracluster gas of the Coma cluster that presents a radio halo, Coma C, with an extension of ~1 Mpc in radius located in the central region of the cluster (Willson 1970). The Lorentz factor of the relativistic electrons, $\gamma \approx 10^4$, is approximately the same for radio and HXR emissions. So, it is very likely that the same electrons produce radio and the hard X-ray emissions. Because of the short lifetimes of the high energy electrons, HXR and radio emission are expected only in clusters with a very recent or current injection of relativistic electrons, probably in clusters with very recent merging activity. Relating the observed synchrotron radio flux to the X-ray IC flux we obtain:

$$f_x = C(\alpha)\ F_r B^{-(1+\alpha)} \nu_r^{\alpha} \epsilon_x^{-(1+\alpha)}$$

where α is the slope of the radio halo spectrum and F_r is the radio flux at the frequency ν_r; for $C(\alpha)$ see Rephaeli (1979).

The value of the radio spectral index is still uncertain for Coma C. Considering all the radio fluxes measured between 30.9 MHz and 1.4 GHz, Kim et al. (1990) and Giovannini et al. (1993) determined a value of $\alpha = 1.34 \pm 0.06$, while $\alpha = 1.16 \pm 0.03$ is obtained using the flux measured at 1.4 GHz by Deiss et al. (1997). We have recently remodeled the radio flux spectrum of Coma C between 30.9 MHz and 2.7 GHz using the data set given in Giovannini et al. (1993), taking into account the electron energy losses due to synchrotron and IC emission (see Fig. 4).

The best-fit indicates an electron injection spectrum of 2.92±0.20 that means $\alpha = 0.96 \pm 0.10$, 90%. A curvature of the radio spectrum appears at $\nu_r > 100$ MHz due to electron ageing. However, the value of the intracluster magnetic field is quite independent from the radio spectral index : B≡ $0.14 - 0.16 \mu G$ for α_r in the range 0.96-1.34. The energy density of the emitting electrons results to be $\sim 7 \times 10^{-14}$ $ergs/cm^3$ using a size of 1 Mpc and a distance of 138 Mpc for the radio halo Coma C.

The nonthermal contribution to the classical 2-10 keV energy range is not lower than 10%. This contribution has implications for the determination of the intracluster gas properties. The thermal flux must be lower and a consequence is that the integrated gas mass is lower with respect to the value derived from a purely thermal model.

The value of the magnetic field derived by the Inverse Compton model seems to be inconsistent with the measurements of Faraday rotation of polarized radiation through the hot ICM that give a line-of-sight value of B in the range $\sim 2 - 6$ $h_{50}^{1/2}$ μG (Kim et al. 1990; Feretti

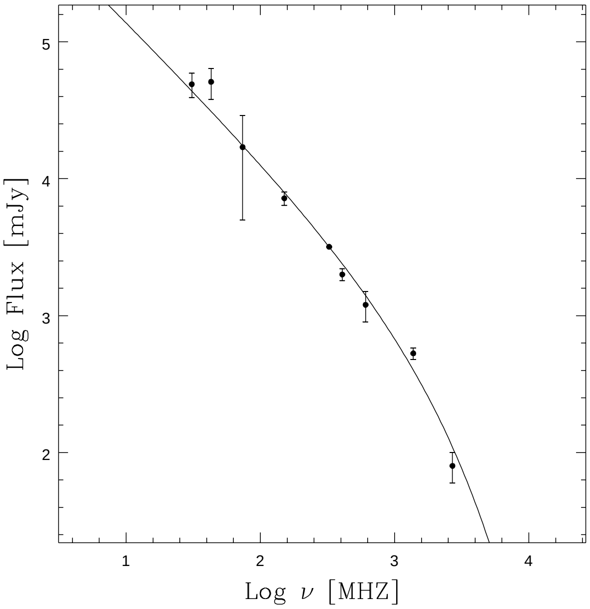

Fig. 4. The radio halo spectrum of Coma C. The best-fit is obtained taking into account the electron energy losses. The χ^2_{red} is 2.78 for 6 d.o.f..

et al. 1995). However, Feretti et al. (1995) inferred also the existence of a weaker magnetic field component, ordered on a scale of about a cluster core radius, with a value of B in the range $\sim 0.1 - 0.2\ h_{50}^{1/2}\ \mu G$, consistent with the value derived using the IC model. So, we can argue that the strongly tangled magnetic field component of 6 μG is likely present in local cluster regions, while the overall cluster magnetic field may be represented by a weaker and ordered component, whose strength is in good agreement with the present estimate. Other determinations (or lower limits) of B based on different methods are in the range 0.2-0.4μG (Hwang 1997; Bowyer & Berghöfer 1998; Sreekumar et al. 1996; Henriksen 1998). In particular, the equipartition magnetic field is $\sim 0.4\ h_{50}^{2/7}\ \mu G$ (Giovannini et al. 1993).

Regarding the origin of the IC magnetic field, it has been suggested that galaxy motion may drives a turbulent dynamo which amplifies faint seed fields to an average value of $\sim 0.1 - 0.2 \mu G$. The seed fields are supplied through gas loss by galaxies (Goldman & Rephaeli 1991; De Young 1992). Larger magnetic fields require different amplification mechanisms, such as merger processes .

3.3. Nonthermal Bremsstrahlung Emission from Suprathermal Electrons

A different interpretation to explain the non-thermal hard X–ray emission has been proposed by Ensslin, Lieu & Biermann (1998). They suggest that the hard excess might be nonthermal bremsstrahlung emission by suprathermal electrons in the ICM. A high energy electron tail is expected by some degree of turbulence present within the medium that accelerates the electrons out of the thermal pool.

3.4. IC Scattering from a Large Population of Cosmic Rays

Another proposed emission mechanism is given by IC scattering of a large population of cosmic rays by the CMB photons (Lieu et al. 1999). In this model the same relativistic component could be also responsible for the soft excess discovered in a few clusters. In particular, for the Coma cluster the extrapolation of the EUV and soft X-ray data (photon index ∼1.75) to the PDS energy range gives a flux only a factor ∼2 lower than the hard excess, suggesting a possible physical connection between the soft and hard excesses. Hovewer, as it has been pointed out by Sarazin (1999), one would not expect a same power law spectrum that fit the HXR and radio emissions and that extends to the EUV emission because the lifetimes of the electrons are very different for HXR/radio and EUV emissions. This may happen only if a large fraction of cosmic ray electrons is generated in an ongoing or very recent strong merger and this should be the case of the Coma cluster where an ongoing merger between the two groups NGC4889 and NGC4874 is likely present in the core of the cluster.

4. Hard X-ray Emission in A2199

The other cluster that seems to show evidence of hard X-ray emission is A2199 (Kaastra et al. 1999).

A2199 is a bright cD-type cluster at z=0.030, with a low galactic hydrogen column density of about $9\times10^{19}\ cm^{-2}$. The cD-galaxy, NGC6166, contains the radio source 3C 338. This cluster has completely different characteristics from the Coma cluster. It shows a cooling flow that is anticorrelated with the presence of a radio halo and the regular X-ray distribution shows no signs of merging activity.

There is a marginal evidence of hard X-ray emission in the PDS. Also the MECS data shows a marginal hardening of the spectrum ar radii beyond $10'$. Probably the presence of hard nonthermal emission in the outermost regions will be better analyzed by observatories as XMM, considering the low gas temperature (∼4.5 keV) of the cluster. It will be very interesting to investigate whether also the hard X-ray emission decreases with the radius more slowly than the thermal emission as observed for the soft excess in this cluster (Bowyer et al. 1998) and others two clusters (A1795, Mittaz, Lieu & Lockman 1998 and A4038, Bowyer et al. 1998). The inverse Compton model naturally explains the increase of this ratio. The IC emissivity is due to collisions between cosmic-ray electrons and CMB photons and therefore is linearly proportional to density;

instead the thermal emission is proportional to the square of the density due to electron-ion collisions. The consequence is that surface brightness of the nonthermal component will decline with radius more slowly than that for the thermal emission.

Whether the marginal evidence of nonthermal emission detected by *BeppoSAX* will be confirmed by further observations and it will result not extended, the central radio source could be responsible of this emission.

5. Hard X-ray emission in A2256

The cluster, showing a radio halo, was observed for ~ 100 ksec by *BeppoSAX* . The data analysis reports a marginal evidence of an emission excess in the PDS spectrum with respect to a purely thermal model of 7.3 keV (David et al. 1993), at a confidence level of $\sim 2.9\sigma$. With the IC model we derive a lower limit of $\sim 0.3\mu G$ for the volume averaged intracluster magnetic field using a radio spectral index of 1.8.

6. Future Observations

The *BeppoSAX* and *RXTE* measurements of hard X-ray emission in the Coma cluster and perhaps in A2199 and A2256 are only first steps to assess the general existence of this new spectral component in clusters. We need to observe other clusters with known extended radio emission or also radio quiet clusters. At this scope, A3667 will be observed with *BeppoSAX* for an exposure time of 150ksec (Fusco-Femiano et al.). The cluster presents a radio relic 30 arcmin off-axis. We have already observed the cluster for 100ksec and the data analysis shows essentially upper limits at a level of 2.4 σ that allow to determine a lower limit for the volume-averaged intracluster magnetic field of 0.25 μG and an upper limit to the electron energy density of 6×10^{-15} erg. A1367 will be observed for 100ksec (Rephaeli & Fusco-Femiano). The cluster is a very suitable object to search for hard X-ray emission because of its closeness and the low gas temperature. Finally, A2319 will be observed for 200ksec with RXTE (Rephaeli & Gruber).

7. Conclusions

The search for hard X-ray emission in clusters of galaxies provide insight into nonthermal phenomena in the intracluster space. Problems as the role of magnetic fields on the cluster dynamical history, origin and nature of intracluster magnetic fields, heating of the gas by cosmic ray particles, origin and propagation mode of cosmic ray electrons can be put on a more quantitative basis. Besides, an improved spectral description of cluster X-ray emission will also result in a more accurate determination of the gas thermal properties.

The next missions, in particular XMM, can give a considerable contribution to the detection of hard nonthermal components especially in clusters with a low average gas temperature.

It appears evident that new perspectives to the study of the astrophysics of clusters of galaxies are given by the detection of soft and hard excesses.

Acknowledgements. I thank A.Malizia and S.Molendi for useful contribution to the preparation of my talk in Ringberg Workshop.

References

[1] Bazzano, A., Fusco-Femiano, R., La Padula, C., Polcaro, V.F., & Ubertini, P. 1984, ApJ, 279, 515
[2] Bazzano, A., et al. 1990, ApJ, 362, L51
[3] Branduardi-Raymont, G., Mason, K.O., Murdin, P.G., & Martin, C. 1985, MNRAS, 216, 1043
[4] Bond, H.E., & Sargent, W.L.W. 1973, ApJ, 185, L109
[5] Bowyer, S., Lieu, R., & Mittaz, J.P.D. 1998, *The Hot Universe: Proc. 188th IAU Symp., Dordrecht-Kluwer, 52*
[6] Bowyer, S., & Berghöfer, T.W. 1998, ApJ, 506, 502
[7] David et al. 1993, ApJ, 227, 364
[8] Deiss, B.M., Reich, W., Lesch, H. & Wielebinski, R. 1997, A& A, 321, 55
[9] De Young, D.S. 1992, ApJ, 386, 464
[10] Dow, K.L. & White, S.D.M. 1995, ApJ, 439, 113
[11] Elvis, M., Plummer, D., Schachter, J., & Fabbiano, G. 1992, ApJ Suppl.Ser., 80,257
[12] Ensslin, T., Lieu, R., & Biermann, P.L. 1998, A&A, 344, 409 astro-ph/9808139
[13] Feretti, L., Dallacasa, D., Giovannini, G., & Tagliani, A. 1995, A&A, 302, 680
[14] Fusco-Femiano, R., Dal Fiume, D., Feretti, L., Giovannini, G., Grandi, P., Matt, G., Molendi, S., & Santangelo, A. 1999, ApJL, 513, L24
[15] Giovannini, G., Feretti, L., Venturi, T., Kim, K.T., & Kronberg, P.P. 1993, ApJ, 406, 399
[16] Goldman, I., & Rephaeli, Y. 1991, ApJ, 380, 344
[17] Henriksen, M. 1998, PASJ, v. 50, 389
[18] Hughes, J.P., Yamashita, K., Okumura, Y., Tsunemi, H., & Matsuoka, M. 1988, ApJ, 327,615
[19] Hughes, J.P., Gorenstein, P., & Fabricant, D. 1988, ApJ, 329, 82
[20] Hughes, J.P., Butcher, J.A., Stewart, G.C., & Tanaka, Y. 1993, ApJ, 404, 611
[21] Hwang, C.-Y. 1997, Science, 278, 1917
[22] Kaastra, J.S. 1999, ApJL, in press
[23] Kim, K.T., Kronberg, P.P., Dewdney, P.E., & Landecker, T.L. 1990, ApJ, 355, 29
[24] Lieu, R., Ip, W.-H, Axford, W.I., & Bonamente, M. 1999, ApJL, 510, L25
[25] Matt, G., et al. 1999 , A&A, 341, L39
[26] Mittaz, J.P.D., Lieu, R., & Lockman, F.J. 1998, ApJ, 498, L17
[27] Rephaeli, Y. 1979, ApJ, 227, 364

[28] Rephaeli, Y., Gruber, D.E., & Rothschild, R.E. 1987, ApJ, 320, 139
[29] Rephaeli, Y., Ulmer, M., & Gruber, D.E. 1994, ApJ, 429, 554
[30] Rephaeli, Y., Gruber, D.E., & Blanco, P. 1999, ApJL, 511, L21
[31] Sarazin, C.L. 1999, ApJ, in press
[32] Sreekumar, P. et al. 1996, ApJ, 464, 628
[33] Watt, M.P., Ponman, T.J., Bertram, D., Eyles, C.J., Skinner, G.K., & Willmore, A.P. 1992, 258, 738
[34] Willson, M.A.G. 1970, MNRAS, 151, 1

Proceedings of the Workshop: *"Diffuse Thermal and Relativistic Plasma in Galaxy Clusters"*
Ringberg Castle, Germany, April 19–23, 1999, eds. H. Böhringer, L. Feretti & P. Schuecker, MPE Report 271, pp. 197-200

Celestial Origin of the Excess EUV Emission in Clusters: Data Analysis Issues

Richard Lieu[1], Massimiliano Bonamente[1], Jonathan P. D. Mittaz[2], Florence Durret[3] and Sergio Dos Santos[3]

[1] Department of Physics, University of Alabama, Huntsville, AL 35899, U.S.A.
[2] Mullard Space Science Laboratory, UCL, Holmbury St. Mary, Dorking, Surrey, RH5 6NT, U.K.
[3] Institut d'Astrophysique de Paris, CNRS, 98bis Bd Arago, F-75014 Paris, France

Abstract. The EUV excess emission from A2199 and A1795 remains a major unexplained astrophysical phenomenon. However, most of the excess was detected at large cluster radii, and since the EUVE Deep Survey (DS) is background limited, the level of inferred emission from these fainter regions is sensitive to the background subtraction method. In this proceedings Bowyer et al. pronounced that in our original papers the background was derived theoretically, and that the true background radial profile mimics that of extended cluster emission, which renders our reported EUV excess erroneous. Here we point out that our critics misunderstood the data analysis procedures which we carefully adopted: we have always avoided sections of the DS detector where background gradients could lead to false detections. We also emphasize the importance of adhering to raw data, and demonstrate how further artificial manipulations, such as usage of the pulse-height thresholding technique, readily explains why our critics grossly mis-evaluated diffuse radiation parameters.

The origin of diffuse EUV and soft X-ray emission from the Virgo and Coma clusters of galaxies (Lieu et al. 1996a,b), detected at a level higher than that expected from the hot intracluster medium (i.e. the cluster soft excess, or CSE, syndrome), has remained unsolved, although it is now plausible that both thermal and non-thermal processes have played a responsible role (Cen & Ostriker 1999, Sarazin 1999, Lieu et al. 1999 and references therein). A much more serious theoretical puzzle, however, is presented by the EUVE data of the rich clusters Abell 1795 and 2199, where the CSE emission was found to be very soft (with luminous EUV excess unaccompanied by any excess in the 1/4-keV band of the ROSAT PSPC) and absent from the cluster centers (Mittaz, Lieu & Lockman 1998; Lieu, Bonamente & Mittaz 1999, hereafter abbreviated as LBM). Non-thermal models have the difficulty of reproducing the extreme CSE softness, which requires the intrinsic spectrum to encompass a large flux at energies $<$ 0.2 keV, with sharp cut-off at $\sim$ 0.2 keV. Thermal models, on the other hand, imply the existence of vast quantities of warm gas at the outer regions of these regular clusters. Partly because of these reasons, some researchers continue to raise pressing questions on the observational integrity of CSE, especially with respect to A1795 and A2199. In particular, an obvious data analysis area worthy of scrutiny is the subtraction of the EUVE detector background, as the inferred signals at large cluster radii, being only a small fraction of the background, are sensitive to this procedure.

To understand the potential problems involved in analysing data from the EUVE DS detector, we first describe the essential aspects of the DS background behavior which can affect the analysis of cluster data. We emphasize that here and after, unless otherwise explicitly stated, only raw data (i.e. the output product of the EUVE standard telemetry processing pipeline, as publically archived) have been employed. The formidable problems which confront usage of additionally manipulated data will be enlisted shortly.

The portion of the DS occupied by the Lex/B (69 - 190 eV) filter is rectangular in shape, and the sensitivity of the detector to background photons and particles is not spatially uniform across this area[1]. In Figure 1 we show contours of the background as obtained by accumulating detector images of three extragalactic pointings, viz. 2EUVE J1100+34.4, 2EUVE J0908+32.6, and M15, totalling an exposure of $\sim$ 85 ksec, comparable to the longest exposure EUVE has in any single observation of an individual cluster. All bright sources have been removed. The figure results from a multi-scale wavelet analysis and reconstruction (see Slezak, Durret & Gerbal 1994) of the detector image, retaining features (in every spatial scale) which have a minimum significance level of 3 σ. It can be seen from Figure 1 that there is no evidence of extended emission at any scale, and that the background exhibits large scale gradients at the extremeties of the y-axis. Note that this spatial pattern is typical of the DS Lex/B background for commensurate exposures. Thus, although such a 2-D view offers firm assurance that cluster glows are inherently not

[1] Note that this sensitivity non-uniformity is *not* a vignetting effect, due to the obvious lack of azimuthal symmetry around boresight

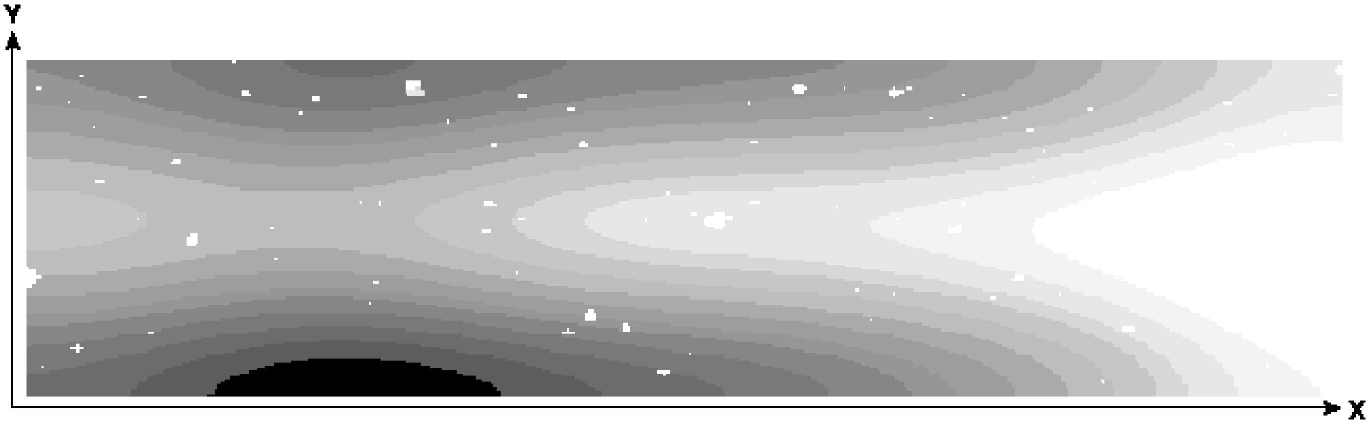

Fig. 1. Figure 1. Greyscale map of the surface brightness of the DS as obtained by co-adding the detector image of three separate pointings (details see text) totalling an exposure of $\sim$ 85 ksec. The contours are scaled linearly between the maximum and minimum brightness values, which differ by 13 %. The normal convention adopted for the detector axes is also indicated.

present in background fields, it also reveals the potential dangers of a 1-D view, viz. that any radial surface brightness profile centered at or near boresight (where clusters are usually observed) could lead to an underestimate of the background if this is taken from an annulus with large (inner and outer) radii which encompasses the bands of lower background.

Nonetheless, a simple way of minimizing this difficulty does exist, and (though not explicitly stated) has been the manner in which analysis leading to our past publications was performed. It involves truncating areas of large and small y coordinate. There are no strict criteria on how to execute this, although a reliable method is to plot the total detector counts as a function of y after they have been summed over all values of x, and place the y-limits at the extreme ends of the 'plateau' region. For the more off-axis pointings, such as our present re-observation of A2199 (when the cluster center is $\sim$ 11.5 arcmin from boresight along the detector +x direction), this invariably leads to well-behaved background profiles, as confirmed *without exception* by analysis of many long exposure fields (Mrk 421, NGC 5548, PKS 2155-304, PSR J0108-1431, and the forementioned three fields, totalling an exposure of 0.736 Msec). To illustrate, we show in Figure 2 the y-profile of the composite detector image of all such pointings, and in Figure 3 the radial profile of the image when events associated with y-coordinates outside the 'plateau' were excluded. The radial profile does not exhibit any systematic downward trend until a radius of $\sim$ 28 arcmin. Thus, e.g., for a cluster which extends to $\sim$ 15 arcmin the usage of the 15 - 28 arcmin region as background would not have led to an under-subtraction problem.

Other potential issues are the use of a template background and the effect of data manipulation. Detailed treatment of this subject is given in Kaastra (1999) but we summarise the main points here. A commonly used technique of 'processing' the raw data, known as *PH thresholding*, attempts to improve the signal-to-noise of an observation by rejecting some of the particle background. One first constructs a PH histogram of the counts detected within a certain region, which consists of a normally distributed peak of photon events superposed upon a linearly sloping continuum of particle events, as illustrated in Figure 4a. By suitably setting the PH limits to select only events within the photon peak, it is possible to reject a good fraction of the particle background without compromising the source signal. While the method works quite well for a point source, using a PH histogram for the source region only, it has serious problems for diffuse emissions be-

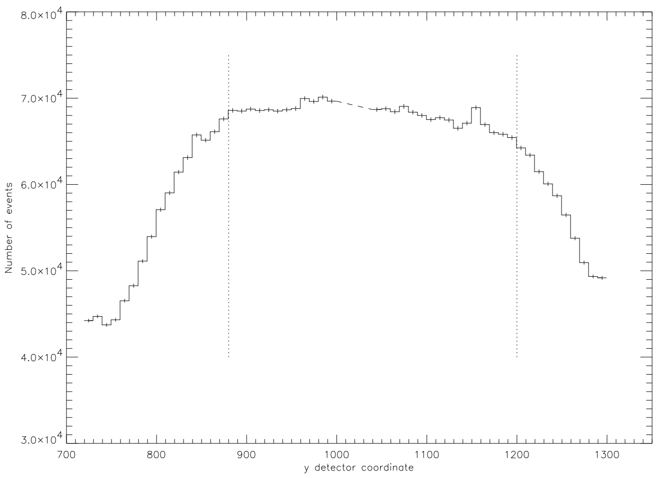

Fig. 2. The intensity distribution of the DS along the detector y-axis, obtained by summing the background counts over all values of x at a given y. The dashed line represents a strip where bright point sources (i.e. the observatory targets) affected the background - this region is therefore not shown. The dotted lines mark those y-limits beyond which the profile steepens considerably. In computing radial profiles only the y pixels within these limits were used. The data were obtained by merging many detector images (see text).

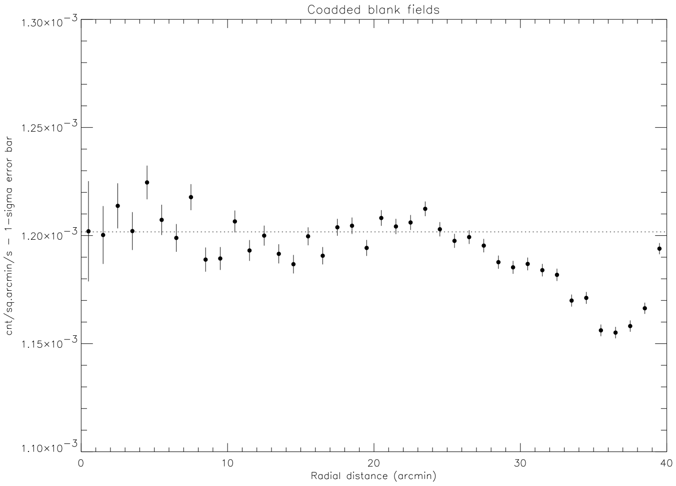

Fig. 3. Radial profile of the same integrated DS detector image as that used to produce Figure 2, with data outside the limits of the y-profile 'plateau' excluded. The center of the annular system coincides with the detector position where the center of A2199 was located during the re-observation of this cluster (i.e. 11.5 arcmin off-axis along the detector +x direction). The dotted line represents the average background computed from the 15 - 28 arcmin region.

cause both the location and width of the photon peak (in PH space) vary substantially across the detector. While Figure 4a shows the distribution at boresight, Figure 4b shows the distribution derived from an outer region, highlighting the change in the PH distribution as a function of position. Specifically, as one moves away from the detector center, the peak of the photon gaussian shifts to higher values and the width increases.

A trivial way of PH thresholding the DS data, often employed to remove detector artifacts due to particle events with small PH values, is to set a lower PH limit using the on-axis PH distribution. This method introduces minimal bias to the data because off-axis photon events, which are peaked at higher PH, are not excluded. The suppression of particle background is, however, not significant until one also sets an upper PH limit. It is important to realize that for diffuse emission analysis the application of a fixed pair of on-axis PH thresholds across an extended region would lead to systematic loss of photons towards larger radii - regions where the thresholds are no longer 'in tune' with the photons (e.g. Figure 4b). The result is a decrease in the thresholded background with radius, an effect which renders background radial profiles appear like clusters (Figure 4c). This is the reason why Bowyer, Berghöfer, and Korpela 1999 (hereafter abbreviated as BBK) recently made the erroneous conclusion that the CSE at the outer regions of A1795 and A2199, *including even the primary radiation of the hot intracluster gas*, are mere background effects. In fact, a map of the spatial distribution of the peak PH value of the photon gaussian (Kaastra 1999) explains precisely why BBK finds much

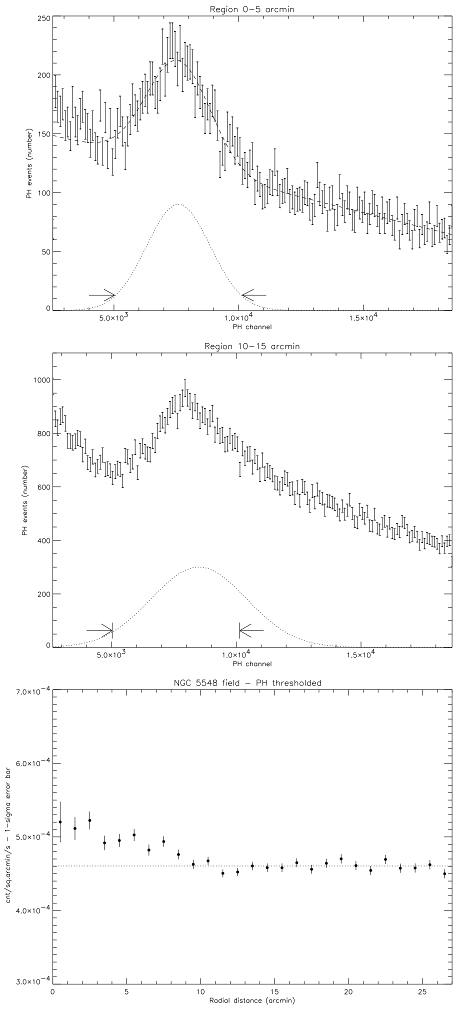

Fig. 4. PH distributions of the DS detector events as collected by a deep exposure (during an observation of NGC 5548). 4a shows the histogram within a circle centered at boresight, and radius 5 arcmin. 3b shows the same for an annulus of inner radius 10 arcmin, outer radius 15 arcmin. Dotted line gives the gaussian photon component of the best-fit model. In 4a the arrows mark the 2 σ limits of this gaussian, while in 4b they mark the locations of the same PH values to highlight how the application of a pair of 'central thresholds' leads to loss of photon events at larger detector radii (where the gaussian has different peak and width). 4c shows a radial profile of this NGC observation, centered at boresight, with PH thresholding applied at the limits of the 0 - 5 arcmin gaussian (i.e. the arrows in 4a and 4b) and detector y-thresholds as in Figures 2 and 3. Note the artificial loss of photons created by this additional data processing results in a profile which mimics cluster detection.

steeper background gradients (relative to the raw data) in certain locations of the DS detector. Therefore, PH thresholding of extended sources compromises data integrity, unless one undertakes the elaborate task of applying position dependent PH limits, as in the case of Kaastra (1999) who also subtracted a template background obtained from blank field pointings at random times and directions. Even after such efforts of Kaastra the meaning of the results is unclear because the heavy data manipulations involved, *coupled with* the usage of a 'foreign' template which is not formed from observations at very different directions and times, raises concerns over the stability of the DS detector regarding the well-known complex and variable behavior of its background - concerns which are not easy to deal with in a totally satisfactory manner.

In conclusion, we elaborated the original data analysis method in respect of background handling. The procedures we adopted, viz., usage of raw data and avoidance of detector areas where background gradients are known to adversely affect radial profiles, do not suffer from an under-subtraction of the detector background. Further, our critics arrive at a different set of results because they performed additional artificial manipulations of the raw data, causing a loss of genuine signals in the case of extended sources.

References

[1] Bowyer, S., Berghöfer, T., & Korpela, E., 1999, *Proc. of workshop on 'Thermal and Relativistic Plasmas in Clusters of Galaxies'*, Schloss Ringberg, Germany, eds. H. Böhringer, L. Feretti, & P. Schuecker.
[2] H. Böhringer (also *astro-ph 9907127*).
[3] Cen, R., & Ostriker, J.P. 1999, *ApJ*, **514**, L1.
[4] Kaastra, J.S., Lieu, R., & Mittaz, J,P.D., 1999, *A & A*, in preparation.
[5] Lieu, R., Mittaz, J.P.D., Bowyer, S., Lockman, F.J., Hwang, C. -Y., Schmitt, J.H.M.M. 1996a, *Astrophys. J.*, **458**, L5–7.
[6] Lieu, R., Mittaz, J.P.D., Bowyer, S., Breen, J.O., Lockman, F.J., Murphy, E.M. & Hwang, C. -Y. 1996b, *Science*, **274**, 1335–1338.
[7] Lieu, R., Ip W.-I., Axford, W.I. and Bonamente, M. 1999, *ApJL*, **510**, 25–28.
[8] Lieu, R., Bonamente, M., & Mittaz, J.P.D. 1999, *ApJ*, **517**, L91.
[9] Mittaz, J.P.D., Lieu, R., Lockman, F.J. 1998, *Astrophys. J.*, **498**, L17–20.
[10] Morrison, R. and McCammon D., 1983, *Astroph. J.*, **270**, 119–122.
[11] Sarazin, C.L. 1999, *ApJ*, in press.
[12] Slezak, E., Durret, F., & Gerbal, D. 1994, *AJ*, **108**, 1996.

Proceedings of the Workshop: *"Diffuse Thermal and Relativistic Plasma in Galaxy Clusters"*
Ringberg Castle, Germany, April 19–23, 1999, eds. H. Böhringer, L. Feretti & P. Schuecker, MPE Report 271, pp. 201-206

A Reanalysis of EUV Emission in Clusters of Galaxies

Stuart Bowyer[1], **Thomas W. Berghöfer**[2] **and Eric Korpela**[1]

[1] Space Sciences Laboratory, University of California, Berkeley, CA 94720-7450, USA
[2] Max–Planck–Institut für extraterrestrische Physik, Giessenbachstraße, 85740 Garching, Germany

Abstract. We report a new analysis of diffuse EUV emission in clusters of galaxies. We find the cluster emission is strongly influenced by the variation of the telescope sensitivity over the field of view and upon the details of the subtraction of the EUV emission from the X-ray plasma. We investigate these effects on Abell 1795, Abell 2199, and the Coma cluster. When we use the appropriate correction factors, we find there is no evidence for any excess EUV emission in Abell 1795 or Abell 2199. However, we do find extended EUV emission in the Coma cluster and in the Virgo cluster using our new analysis procedures, confirming that in at least these clusters some as yet unidentified process is operative.

1. Introduction

Extreme ultraviolet (EUV) emission in excess of that produced by the well-studied X-ray emitting gas in clusters of galaxies has been reported in five clusters of galaxies. The effective bandpass of the EUVE telescope employed in these observations is defined by the intrinsic response of the telescope combined with the absorption of the intervening galactic interstellar medium (ISM). This bandpass has a peak at 80Åwith 10% transmission at 66 and 100Å. A variety of instrumental effects that might have explained these results have been advanced but a detailed analysis has shown these factors cannot explain the data (Bowyer, Lieu & Mittaz, l998).

It is interesting to note that the EUV excess is detected in some ROSAT images. However, the effect is sufficiently marginal that the ROSAT results can almost be explained away through the use of particular combinations of intervening Galactic ISM and its ionization state, and different cross sections for absorption by hydrogen and helium (Arabadjis & Bregman, 1999). The EUVE results, however, cannot be explained in this manner. It is also interesting to note that the EUV excess has been reported in every cluster investigated with EUVE.

A number of suggestions have been made as to the source of this EUV emission. Initial work focused on additional components of "warm gas" ($\sim 10^6$ K). The problem with this suggestion is that gas at this temperature is near the peak of the cooling curve and substantial energy is needed to supply the energy radiated away. One mechanism that can provide this energy is gravitational condensation. Cen & Ostriker (1999) have suggested that a pervasive warm intergalactic gas constitutes the majority of matter in the Universe; as this gas coalesces onto clusters of galaxies, it could produce the energy needed to sustain the EUV emitting gas.

Several authors (Hwang, 1997; Enßlin & Biermann, 1998) have suggested the EUV flux in the Coma Cluster is inverse Compton (hereafter: IC) emission produced by the population of electrons producing the radio emission scattering against the 3° K Black Body cosmic background. However, Bowyer & Berghöfer (1998) have shown that the existing population of radio emitting cosmic ray electrons cannot be responsible for the EUV emission in the Coma cluster, and some other population of cosmic rays will be required if this mechanism is the source of the EUV emission in this cluster. Lieu et al. (l999a) have suggested that the Coma cluster contains a large population of cosmic rays which are producing the 25 to 80 keV emission seen by BeppoSAX (Fusco-Femiano et al., 1999) and RXTE (Rephaeli, Gruber & Blanco 1999) via IC emission. They propose this population of cosmic rays extrapolated to lower energies will produce the observed EUV flux by IC emission. However, these authors have not addressed the fact that this population of electrons will produce a spatial distribution of the EUV flux which is inconsistent with the observational results of Bowyer & Berghöfer (1998).

Enßlin, Lieu, & Biermann (l999) have explored processes that might produce a heretofore undetected population of lower energy cosmic rays which could produce this flux. They demonstrate an evolutionary scenario in which relativistic electrons produced in the last merger event in Coma two Gyrs ago could produce these electrons. However, this model cannot produce the spatial profile of the EUV emission obtained by Bowyer & Berghöfer. They also consider IC scattering of starlight photons and show that under some scenarios this could account for the EUV flux and the required spatial distribution.

Sarazin & Lieu (1998) have suggested that all clusters of galaxies may contain a relic population of cosmic ray electrons that are unobservable in the radio and these will produce excess EUV flux by inverse Compton scattering against the 3° K cosmic background. Their proposal is based upon, and explains, details of the EUV data obtained on Abell 1795 (Mittaz, Lieu & Lockman, 1998).

We have obtained new data on some of these clusters and have analyzed archival data on others. We find that the results obtained are crucially dependent upon the characterization of the DS telescope, and upon details of the estimation of the EUV emission from the X-ray plasma. The results we obtain are quite different from those obtained in previous work.

2. Data and Data Analysis

All data were processed using procedures of the IRAF EUV package provided by the Center for EUV Astrophysics (CEA, Berkeley) which were especially designed for the analysis of EUVE data. As part of this process, we excluded detector events with pulse heights far from Gaussian peak of the photon pulse-height spectrum. Low energy events due to spurious detector noise($\approx$15% of the total), and high energy counts due to cosmic rays and charged particles ($\approx$25% of the total), were screened out. A detailed description of different background contributions to the DS data can be found in Berghöfer et al. (1998). We point out that the location of the Gaussian peak in the pulse-height spectrum is not constant for all EUVE DS observations since the gain of the DS detector was changed periodically in the course of the mission. Consequently, pulse height limits were chosen individually for each DS observation.The resulting filtered event lists were corrected for electronic deadtime and telemetry throughput effects.

The background of the DS telescope consists of a uniform detector background, $B_{\rm int}$, and a component that may vary over the field because of a variety of effects including vignetting, variations in the thickness of the filter covering the detector face, variations in the quantum efficiency over the face of the detector, and other causes. Hereafter we call this second component the vignetted background, $B_{\rm vig}$. To investigate the possibility of a field variation effect, we chose four 20,000 s observations of blank sky with low and similar backgrounds that were obtained in a search for EUV emission from nearby pulsars (Korpela & Bowyer, 1998). We added 90,000 s of data from a blank field at R.A.$_{2000}$ = $3^h31^m39^s$, Dec.$_{2000}$ = $+18°28'33''$ obtained from the EUV archives. *We emphasize that the images were added in detector coordinates, NOT sky map coordinates.* We processed the data as described above. We established that once proper pulse height selection of the detector events had been made, the detector backgrounds were all spatially identical.

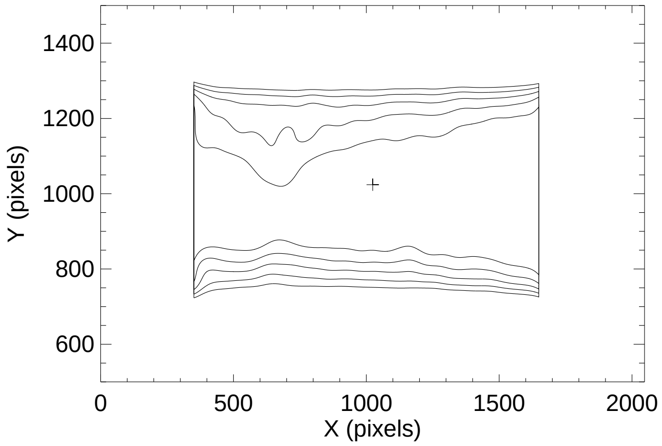

Fig. 1. A contour plot of counts obtained in long duration DS exposures showing the sensitivity variation of the DS Telescope over the field of view. We have cut the regions at the detector ends where the detector distortion becomes severe. The field displayed is approximately 1.75 degrees x 0.73 degrees.

A contour plot of normalized count rates in these exposures convolved with a 32 pixel wide Gaussian is shown in Figure 1. The contours represent a 10% change in the measured count rates. [1] It is informative to compare this observationally derived result with the theoretically derived product provided in Sirk et al. (1997), which has been used in previous work on EUV emission clusters.

All observations contain both $B_{\rm int}$ and $B_{\rm vig}$. Because the ratio of these two backgrounds can vary, we must correct for this effect when scaling previously measured backgrounds to the backgrounds of our observations. Our background subtracted image is:

$$I_{\rm net} = I_{\rm on} - B_{\rm int} - fB_{\rm vig} \quad (1)$$

where $I_{\rm on}$ is the on-source image. The term $B_{\rm int}$ is derived from measurements of the background in obscured regions of the detector covering about 3.5 % of the detector area. The term $B_{\rm vig}$ represents the vignetted background. The factor f is used to fit the vignetted background levels in the blank field with those of the on-source image. This factor is derived by fitting the observed photonic background with that of the blank field images in a region far from the source, $R > 15'$ in the case of Abell 1795 and Abell 2199, and $R > 17'$ in the case of the Coma Cluster. Because of the long duration of the background exposures, the statistical errors in f are less than 1%. When comparing on-source and background in small detector regions, our errors are dominated by the count statistics of the region, rather than errors in the background fitting.

We have compared new data on Abell 1795 with the archival data on this cluster and find that the new results

[1] Investigators interested in using this observationally derived sensitivity plot may access Fits Files at “http://sag-www.ssl.berkeley.edu/~korpela/euve_eff” .

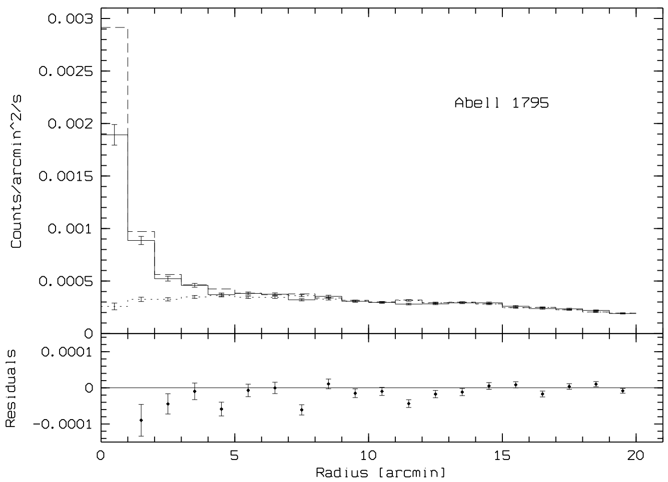

Fig. 2. The azimuthally averaged radial intensity profile of the EUV flux in Abell 1795 is shown as a solid line. The vignetted background from long observations of blank fields is shown as a dotted line. There is no excess EUV emission beyond $4'$.

at $R > 2'$ (which excludes the effects of a bright transient source in the new data set) are identical within the counting errors, confirming the validity of the original data set used by Mittaz et al. (1998). Because the two data sets are identical and the more recent set is contaminated with a point source, we have used the archival data on Abell 1795 for our subsequent analysis.

We derived the azimuthally averaged radial intensity profile of the EUV emission of the cluster as a function of projected radius from the central core assuming spherical symmetry. The results are shown in Fig. 2. Our vignetted background is shown as a dotted line. It is visually apparent that there is no excess EUV emission at radii larger than $4'$. It is also clear that an improperly chosen background chosen at $R > 15'$ would result in apparent emission at smaller radii simply because of the effects of the vignetted background in the DS telescope.

We next determined the expected intensity and distribution of the EUV emission expected from the X-ray emitting plasma. We used the X-ray radial emission profile provided by Briel & Henry (1996). This profile was derived from ROSAT PSPC observations of the cluster in the energy band between 0.5–2.4 keV. At larger radii ($R > 4'$) this profile is well fit by a King profile (1972) with $\beta = 0.93$ and describes the large scale cluster X-ray emission with a temperature of 6.7 keV. The ROSAT observations also show a central excess emission within $R < 4'$. Briel & Henry (1996) obtained a temperature of 2.9 keV for this excess. We derived conversion factors for counts in the 0.5–2.4 keV band of the ROSAT PSPC to EUVE DS counts using these plasma temperatures. Our derivation employed the MEKAL plasma emission code with abundances of 0.3 solar. For a temperature of 6.7 keV we obtained a conversion factor of 126; the value for 2.9 keV was 110. We found that varying the temperature by ± 1 keV or using different abundances only affect these conversion factors by a few percent and thus changes of this nature would not significantly alter our results. We found that a deprojection of the emission components which takes into account the emission measures and sizes of the different components leads to the same result.

The correction for the intervening absorption of the ISM in our Galaxy will have a substantial impact on our results. Many workers simply apply the cross sections of Morrison & McCammon (1983) or Balucińska-Church & McCammon (1992) for this correction, but there are several problems with this approach. The HeI absorption coefficient in this work is incorrect (Arabadjis & Bregman 1999). In addition, the ionization state of the ISM will substantially affect the result. The ISM absorption at EUV energies is primarily due to HI , HeI , and HeII ; the metals in the list of Balucińska-Church & McCammon (1992) provide less than 30% of the absorption at wavelengths greater than 50 Å and less than 10% at wavelengths greater than 100 Å and none of the Galactic ISM is in the form of HeIII (see discussion below). Hence in general terms the absorbing material and related factors are given by:

$$N(\mathrm{H(tot)}) = N(\mathrm{HI}) + N(\mathrm{HII}) \tag{2}$$

$$N(\mathrm{HeI}) = \frac{1}{10}\,[N(\mathrm{H(tot)})]\,(1 - X(\mathrm{HeII})) \tag{3}$$

$$N(\mathrm{HeII}) = \frac{1}{10}\,[N(\mathrm{H(tot)})]\,(X(\mathrm{HeII})) \tag{4}$$

We have calculated the Galactic ISM absorption using these columns with HI cross sections of Rumph et al. (1994), HeI cross sections from Yan et al. (1998), and HeII cross sections from Rumph et al. We used these values with an improved estimate of the Galactic neutral hydrogen column density in the direction of Abell 1795 of N(HI) = $0.95 \times 10^{20}\mathrm{cm}^{-2}$ (J. Lockman, private communication) . We assume the total helium is 10% of the total hydrogen column. A direct measurement of the HII column can be obtained, in principle, from measurements of the Hα flux in this direction (Reynolds et al. , 1998). Unfortunately, only an upper limit to this flux of $1 \times 10^{19}\mathrm{cm}^{-2}$ is currently available (Haffner, private communication). A reasonable estimate for the HII column, based on all the available data, is that it is close to this upper limit (Reynolds, private communication). Consequently we have used this value for the HII column. The amount of HeII in this direction can be obtained from Fig. 1 of Bowyer et al. (1996). For A1795, $N(\mathrm{H(tot)}) = 1.1N(\mathrm{HI})$, $N(\mathrm{HeI}) = 0.1[1.1N(\mathrm{HI})](1 - 0.02) = 0.108N(\mathrm{HI})$, and $N(\mathrm{HeII}) = 0.1(1.1N(\mathrm{HI})] \times 0.02 = 2.2 \times 10^{-3}N(\mathrm{HI})$. The absorption corrected results are shown in Figure 2. The observed EUV emission is *less* than that produced by the X-ray plasma. This appears to be unphysical but is simply understood as discussed below.

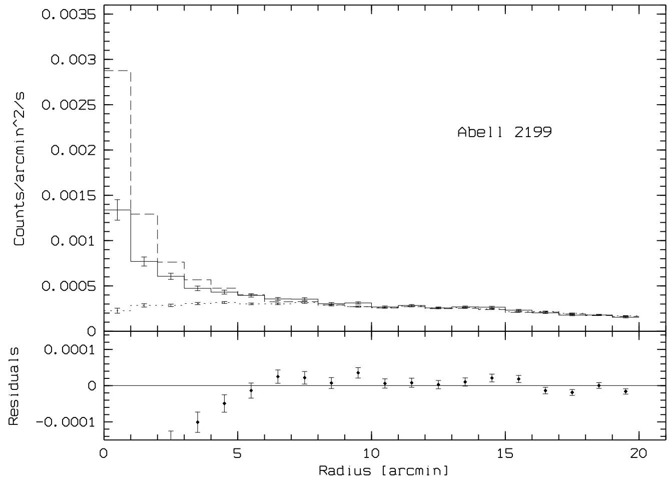

Fig. 3. The azimuthally averaged radial intensity profile of the EUV emission in Abell 2199 is shown as a solid line. The dotted line is the vignetted background. There is no EUV emission beyond $8'$.

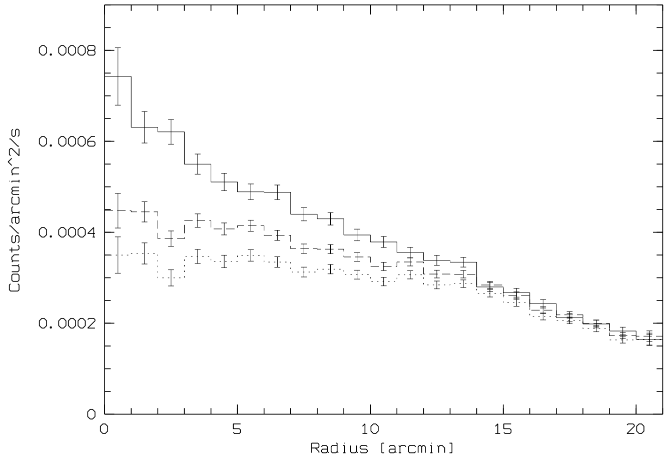

Fig. 4. The azimuthally averaged radial intensity profile of the EUV flux in the Coma cluster is shown as a solid line. The expected EUV emission from the X-ray plasma is shown as a dashed line. The vignetted background is shown as a dotted line.

After taking into account the vignetting and the EUV emission from the X-ray plasma, we see no excess EUV emission in this cluster.

We also examined archival data on Abell 2199 to ascertain whether a vignetted background could have produced an artificial extended diffuse EUV halo in this cluster. In Figure 3 we show the radial profile of the raw EUV data and the vignetted background. It is apparent that there is no excess EUV emission beyond 8 $'$. We use the results of Siddiqui, Stewart, and Johnstone, (1998) to model the EUV emission from the X-ray gas in the cluster. They found T(core) = 2.9 keV and T(outer) = 4.08 keV. The conversion of the ROSAT X-ray profile into EUVE DS count rates has been done as described for Abell 1795. For Abell 2199 we found DS to PSPC hard band count rate ratios of 83.2 for T = 2.9 keV and 89.4 for T = 4.08 keV. Absorption by the Galactic ISM was accounted for using $N(HI) = 8.3\times10^{19}$ (Lieu et al. 1999) with ionization fractions and cross sections as described previously. The results are shown in Figure 3 as a dashed line. Again, the expected EUV emission from the X-ray gas is larger than the observed flux, and there is no excess EUV emission in this cluster.

Finally, we re-examined the previously reported EUV excess in the Coma Cluster. We carried out our analysis using both of the existing DS images of this cluster. Because of the different roll orientation and pointing position in these images, it was necessary to carry out our analysis on each image individually. The results were then summed and the EUV emission and vignetted background are shown in Figure 4 as a solid and dotted line respectively. In this figure, we have fit the vignetted background to the Coma observations beyond $17'$; however, because faint emission due to the cluster likely extends past this point, especially in the direction of the NGC 4874 subcluster, this is likely to be a slight overestimate of the background and hence the excess EUV emission we derive may be a slight underestimate. If the X-ray profile of the Coma Cluster is used as a guide, we expect this effect to be small compared to the statistical errors in each radial bin.

The X-ray profile has been constructed using ROSAT PSPC archival data of Coma. We verified that our PSPC hard band cluster profile is consistent with the profile provided by Briel, Henry & Böhringer (1992) but includes the central excess associated with the galaxy group around NGC 4874. We assumed that this X-ray emission is due to a plasma at T = 9 keV (Donnelly et al., 1999) absorbed by a hydrogen column of 8.7×10^{19}cm^{-2} (Lieu et al., 1996) with ionization fractions and cross sections for Galactic absorption as described above. Here we obtained a DS to PSPC hard band conversion factor of 112.

The residual EUV emission in excess of the expected contribution of the X-ray gas shown in Figure 5 demonstrates that there is, indeed, excess EUV emission in the Coma cluster.

Based on our new analysis technique we also confirm excess EUV emission in the Virgo cluster of galaxies. Details are provided in Berghöfer & Bowyer (this workshop). In Figure 6 we provide a plot of the excess EUV emission in the central part of the Virgo cluster. Clearly, there is EUV emission in excess of the expected low energy tail of the X-ray emitting gas in Virgo.

3. Discussion

The results of our new analysis show no excess EUV emission at radii larger than $4'$ for Abell 1795 and $8'$ for Abell 2199 contrary to previous work on these clusters. When we consider the inner regions for these clusters, we find

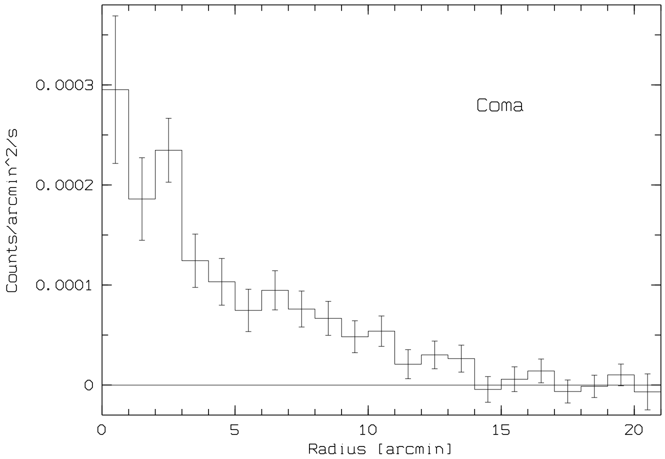

Fig. 5. The excess EUV emission in the Coma cluster.

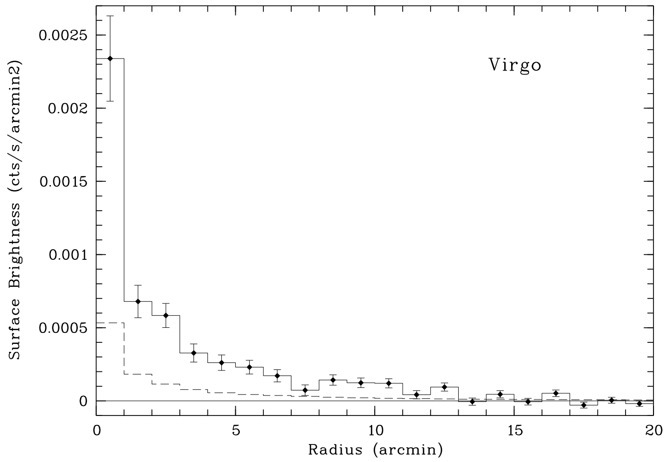

Fig. 6. The excess EUV emission in the center of the Virgo cluster (solid line) in comparison to the expected contribution of the X-ray emitting cluster gas (dashed line).

the results expected are dependent upon a proper evaluation of the EUV emission from the X-ray plasma. When this emission is properly accounted for, the expected EUV emission from the X-ray plasma is *less* than is actually produced. This can be understood in terms of excess absorption within the cluster core. This effect has been noted in studies of X-ray cluster emission in cooling flows, where it is often reported that the hydrogen column density is larger in the core of the cluster. There is no observational evidence for more hydrogen in these regions, and neutral hydrogen is not expected in this environment. A reasonable explanation for this effect is that the X-ray reduction codes employed in these analyses require more absorption for a reasonable fit, and this is achieved blindly by adding more hydrogen with a standard admixture of non-ionized metals. It is more likely that in the cooler regions of the cooling flow, some metals are not completely ionized and these ions produce the extra absorption of the X-ray flux (Allen et al. 1996). This absorption would be even more substantial for the EUV flux, and would produce the effects seen. We point out that a study of the differing amount of absorption in the EUV and X-ray bands may provide sufficient information to identify the primary absorbing species.

When we employ our new analysis techniques with the data on the Coma cluster we find there *is* excess EUV emission confirming the results of previous studies. However, the distribution of this flux differs in detail from that previously reported. The distribution of this radiation is shown in Figure 5, along with the count rate intensity. The intensity in physical units is (slightly) dependent upon the assumed spectral distribution of the flux. A source with a photon spectral index of 1.6 results in an EUV source luminosity of $1.5 \pm 0.5 \times 10^{42} \mathrm{erg\,s^{-1}}$.

It is useful to consider why our results are different from those of Mittaz et al. (1998), and Lieu, Bonamente & Mittaz (1999). While it is difficult to evaluate the details of another researchers' analysis, it is clear that a key difference is our use of an observationally derived vignetted background. Mittaz et al. and Lieu et al. used the theoretical background function (Richard Lieu, private communication) which is essentially flat. In addition, these authors also carried out their analysis of the EUV flux without first removing the non-photonic background from their data. The extent to which this affects the results is not substantial, as we obtain the same general picture with data that has not been processed in this manner. Their approach to estimating the EUV emission produced by the X-ray plasma is also different than ours.

It is interesting to ask why both the analyses of Lieu et al and that presented here do show excess diffuse EUV emission in the Coma cluster and the Virgo cluster. The primary explanation is that both of these clusters do, in fact, have excess EUV emission. This emission is sufficiently extended that the effects of the vignetted background, though changing the details of the results, do not dominate as they do in Abell 1795 and Abell 2199.

Finally, we have examined the effects of fine grained detector variations on the data obtained from any point in the sky. As one example in Fig. 7 we show variations in the blank field image for a $15'$ field of view centered upon the detector coordinates where the EUVE observation of A 2199 was made. The image has been smoothed to $2'$. Count statistics give expected uncertainties of 2.6%. The contours are 90%, 100% and 110% of the mean and are separated by 3.8 σ. A wavelet analysis of this data as presented by Richard Lieu (this conference) would obviously show substantial effects, which would be entirely due to this fine scale structure in the detector. This structure varies over the face of the detector. Consequently the image taken at different locations will be different, which will tend to confuse uncareful workers.

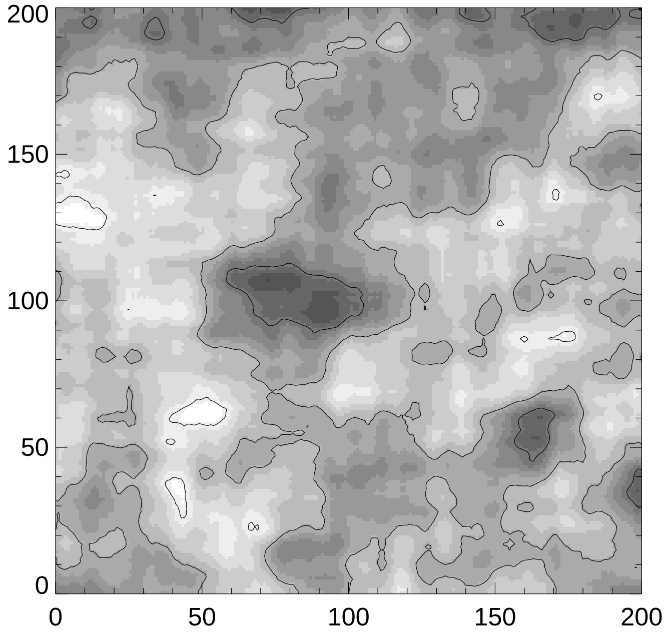

Fig. 7. Variations in the blank field image for a 15′ field of view centered upon the detector coordinates where the EUVE observation of A 2199 was made. The background was smoothed to 2′. Gaussian count statistics give expected uncertainties of 2.6%. The contours are 90%, 100%, and 110% of the mean and are each separated by 3.8σ.

4. Conclusions

We investigated the effects of the telescope sensitivity variation over the field of view and found this was a key factor in investigating extended EUV emission in clusters of galaxies. Our study shows why excess EUV emission has been found in every cluster examined to date with EUVE. *Any* point in the sky will show extended EUV emission using the analysis employed in previous studies of clusters of galaxies. We also used a detailed approach to the evaluation of the EUV flux produced by the X-ray gas in the core regions of these clusters.

We find no evidence for excess EUV emission in Abell 1795 or Abell 2199. We do, however, confirm extended EUV emission in the Coma cluster and Virgo cluster although the distributions of these fluxes are different in detail from that previously reported. The fact that we do find extended EUV emission in the Coma cluster and Virgo cluster using our new analysis procedures confirms that an unidentified processes is operative in this cluster.

Acknowledgements. We acknowledge useful discussions with Michael Lampton, Pat Henry, John Vallerga, Carl Heiles, Richard Lieu, John Mittaz and Jean Dupuis. This work was supported in part by NASA contract NAS 5-30180. TWB was supported in part by a Feodor-Lynen Fellowship of the Alexander-von-Humboldt-Stiftung.

References

[1] Allen, S., Fabian, A., Edge, A., Bautz, M., Furuzawa, A., & Tawara, Y. 1996, MNRAS, 283, 263
[2] Arabadjis, J. S. & Bregman J. N., 1999, ApJ, 514, 607
[3] Balucińska-Church, M. & McCammon, D. 1992, ApJ, 400, 699
[4] Berghöfer, T. W., Bowyer, S., Lieu, R. & Knude, J. 1998, ApJ, 500, 838
[5] Bowyer S., Lampton M. & Lieu, R. 1996, *Science*, 274, 1338
[6] Bowyer S., Lieu, R. & Mittaz, J. P. 1997, IAU Symposium No. 153: The Hot Universe, eds. K. Koyama et al., Dortrecht: Kluwer, 185
[7] Bowyer,S. & Berghöfer, T. W. 1998, ApJ, 506, 502
[8] Briel, U. G., Henry, J. P. & Böhringer, H. 1992, A&A, 259L, 31
[9] Briel, U. & Henry, J. P. 1996, ApJ, 472, 131
[10] Cen, R. & Ostriker, J. 1999, ApJ, in press
[11] Donnelly, R. H., Markevitch, M., Forman, W., Jones, C., Churazov, E. & Gilfanov, M. 1999, ApJ, in press
[12] Enßlin, T. & Biermann, P. 1998, A&A, 330, 96
[13] Enßlin, T., Lieu, R. & Biermann, P. 1999, A&A, 344, 409
[14] Fusco-Femiano, R., Dal Fiume, D., Feretti, L., et al. 1999, ApJ, 513, L21
[15] Hwang, C.-Y. 1997, *Science*, 278, 1917
[16] King, I. 1972, ApJ, 174, L123
[17] Korpela,E. & Bowyer S. 1998, ApJ, 115, 2551
[18] Lieu, R., Mittaz, J., Bowyer, S., et al. 1996, Science, 274, 1335
[19] Lieu, R., Ip, W-H., Axford, W. & Bonamente, M. l999, ApJL, 510 , L25
[20] Lieu, R., Bonamente, M. & Mittaz, J. 1999, ApJ, in press
[21] Mittaz, J., Lieu, R. & Lockman, F. l998, ApJL, 498, L17
[22] Morrison, R. & McCammon, D. 1983, ApJ, 270, 119
[23] Rephaeli, Y., Gruber, D. & Blanco, P. 1999, ApJ, 511, 21
[24] Reynolds, R. J., Tufte, S. L., Haffner, L. M., Jaehnig, K., & Percival, J. W. 1998, Pub. Astron. Soc. Aus., 15, 14
[25] Rumph, T., Bowyer, S. & Vennes, S. 1994, AJ, 107, 2108
[26] Sarazin, C. & Lieu, R. l998, ApJ, 494, L177
[27] Siddiqui, H., Stewart, G. & Johnstone, R. 1998, A&A, 334, 71
[28] Sirk, M. M., Vallerga, J. V., Finley, D. S., et al. 1997, ApJS, 110, 347
[29] Yan, M., Sadeghpour, H. & Dalgarno, A. 1998, ApJ, 496, 1044

Proceedings of the Workshop: *"Diffuse Thermal and Relativistic Plasma in Galaxy Clusters"*
Ringberg Castle, Germany, April 19–23, 1999, eds. H. Böhringer, L. Feretti & P. Schuecker, MPE Report 271, pp. 207-211

EUVE Observations of Clusters of Galaxies: M87

Thomas W. Berghöfer[1], Stuart Bowyer[2] and Eric Korpela[2]

[1] Max–Planck–Institut für extraterrestrische Physik, Giessenbachstraße, 85740 Garching, Germany
[2] Space Sciences Laboratory, University of California, Berkeley, CA 94720-7450, USA

Abstract. We present results of a re-analysis of archival EUVE data of the central region of the Virgo cluster. We employ the new analysis method developed by Bowyer, Berghöfer & Korpela (1999) and find diffuse emission reaching out to a distance of $\approx 13'$. The spatial distribution of this flux is incompatible with a thermal plasma origin. We investigate whether this emission is due to inverse Compton scattering of relativistic electrons against the 3° K black-body background. We show that this emission cannot be produced by an extrapolation to lower energies of the observed synchrotron radio emitting electrons and an additional component of low energy relativistic electrons is required.

1. Introduction

Observations with the *Extreme Ultraviolet Explorer* (EUVE) have provided evidence that a number of clusters of galaxies produce intense EUV emission. However, a variety of alternative explanations have been advanced which dismiss these results. Most recently, Arabadjis & Bregman (1999) argue that in some clusters the EUV excess can be explained away by a different cross section for absorption by hydrogen and helium in the foreground ISM column. Bowyer, Berghöfer & Korpela (1999) find that in some clusters this may explain some excess present in the ROSAT PSPC data, however, this cannot explain the intense EUV excesses reported with EUVE data.

Bowyer, Berghöfer & Korpela (1999) reexamined EUVE data of the clusters Abell 1795, Abell 2199, and Coma. They demonstrate that the initially reported results are based on an improper background subtraction. In previous analyses a flat background has been assumed. However, a detailed investigation of blank field observations with the EUVE Deep Survey (DS) instrument shows that the background consists of two independent components, a non-photonic background which is assumed to be constant over the entire detector field and a background due to photons. The non-photonic background level can be determined in obscured regions of the detector and can be directly subtracted from the raw data. However, the photonic background is affected by telescope vignetting and must be treated differently.

In this paper we employ our new reduction method to EUVE archival data of the central part of the Virgo cluster. We compare our results with results derived from radio observations of this region. Finally, we consider the possibility that the observed diffuse EUV excess emission is due to an inverse Compton process of the known population of relativistic electrons in the ICM near M87.

2. Data and Data Analysis

The Virgo cluster has been observed for 36,000 s with the Deep Survey (DS) Telescope of EUVE (Bowyer & Malina, 1991). Data reduction was carried out with the EUVE package built in IRAF which is especially designed to process EUVE data.

In order to reduce the non-photonic (non-astronomical) background contribution to the scientific data we investigated the pulse-height spectrum of all detected events. A large number of EUVE DS observations of all kinds of astronomical targets has shown that a typical pulse-height spectrum consists of two components, a Gaussian profile representing the source events and an exponential background distribution. More details about the different background contributions to the DS data and the method of pulse-height thresholding can be found in Berghöfer et al. (1998). Here we screened out all events with pulse heights below 5300 ($\approx$15% of the total) and above 13500 ($\approx$26% of the total). From our experience with stellar and extragalactic observations with EUVE we know that this pulse-height selection effectively reduces the non-astronomical background in the data without any significant reduction of the source signal. The effect on the source signal is estimated to be lower than 4%.

Then we applied corrections for detector dead time and primbsching to the screened event list and produced a DS EUV image of the Virgo cluster. We then determined the remaining non-photonic background level in the image from highly obscured regions at the outer most parts of the field of view near the Lexan/B filter frame bars. This non-astronomical background contribution is assumed to be

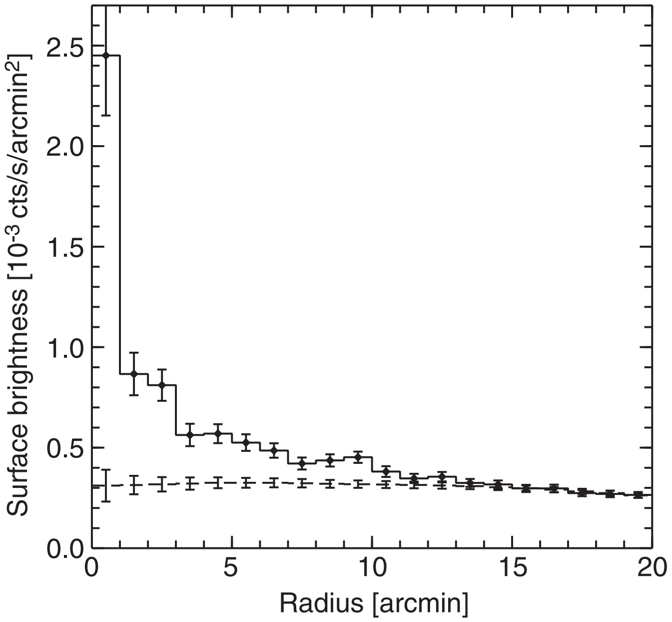

Fig. 1. The azimuthally averaged radial intensity profile of the EUV emission in the central part of Virgo (centered on M87) is shown as a solid line. The dashed line is the vignetted background. There is no EUV emission beyond $\approx 13'$.

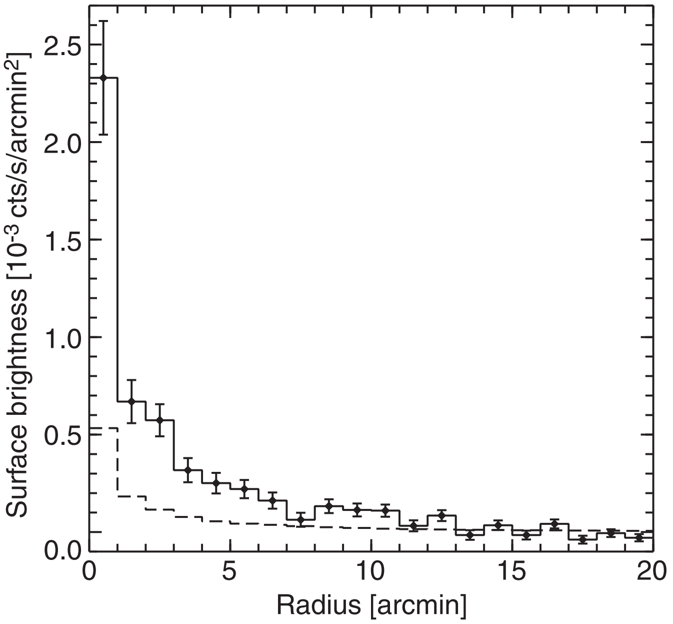

Fig. 2. The solid line shows the azimuthally averaged radial intensity profile of the background subtracted EUV emission in the central part of Virgo. The dashed line provides the contribution of the low energy tail of the X-ray emitting intracluster gas. The central $1'$ bin is dominated by the core and jet in M87 and must be ignored in the context of diffuse emission.

constant over the entire detector field and was subtracted from the image.

In order to subtract the (vignetted) photonic background we computed the azimuthally averaged radial emission profile centered on M87. We used the EUVE DS sensitivity map provided by Bowyer, Berghöfer & Korpela (1999) to determine a radial sensitivity profile centered on the detector position of M87. This was the fit to the outer part (15–20$'$) of the radial emission profile to determine the scaling factor between sensitivity profile and the photonic background in the data. The radial emission profile and the best fit background model are shown in Figure 1. The sensitivity map has been multiplied by the best fit scaling factor and subtracted from the DS image.

3. Results

Figure 1 demonstrates the presence of diffuse EUV emission in the vicinity of M87 which extends to a radius of $\approx 13'$. At larger radii the radial profile is well fit by the background model demonstrating the absence of any significant astrophysical signal. The initial publication on the diffuse EUV emission from Virgo (Lieu et al. 1996) claimed to detect excess emission to $20'$.

In Figure 2 we plot the background subtracted radial EUV emission profile (solid line). The dashed line shows the expected EUV emission of the low energy tail of the X-ray emitting diffuse intracluster gas as derived in the following. Note that the inner $1'$ bin is dominated by the core and jet of M87 and must be ignored for the discussion of the diffuse emission. To determine the diffuse X-ray contribution to the observed EUV emission we processed ROSAT PSPC archival data of the Virgo cluster. We used standard procedures implemented in the EXSAS software package to produce an image from the photon event list. Then a vignetting corrected exposure map has been computed for this data set and a PSPC count rate image was generated by dividing the PSPC image by the exposure map.

We point out that the background in the ROSAT PSPC hard energy band is dominated by the photonic (vignetted) background and the contribution of the non-photonic background is minor. Therefore, a similar analysis as described for the EUVE DS data including a separation of the photonic and non-photonic background contributions is not essential. However, in the case of detectors with low effective areas (e.g., BeppoSAX), and less efficient rejection mechanisms for non-photonic events the background contribution must be treated separately.

For our analysis of the ROSAT PSPC data we selected only photon events in the hardest energy band, channels 90–236. This channel selection has several advantages: First, a contamination by a possible steep spectrum source at soft X-ray energies is excluded and, therefore, ensures that this band pass represents only thermal contributions to the overall diffuse emission in Virgo. Second, this part of the ROSAT band pass is almost uneffected by interstellar absorption. This minimizes errors due to possible differential ISM absorption effects when modeling theoretical conversion factors between DS and PSPC counts.

Third, the count rate conversion factor between DS and PSPC is almost temperature independent in the range of X-ray temperatures measured in the central Virgo region and, thus, ROSAT count rates of the diffuse X-ray emission can be converted into DS count rates by using one single conversion factor.

In order to be able to convert PSPC counts into DS counts we modeled conversion factors for a range of plasma temperatures (0.1–2.7 keV) employing the MEKAL plasma emission code with abundances of 0.34 solar (Hwang et al. 1997). These calculations include absorption by the interstellar medium. We used an ISM absorption column density of $1.72 \times 10^{20}\mathrm{cm}^{-2}$ (Hartmann & Burton 1997) and an absorption model including cross sections and ionization ratios for the ISM as described in Bowyer, Berghöfer & Korpela (1999). In Figure 3 we show the DS to PSPC conversion as a function of plasma temperature. As can be seen, for a wide range of temperatures (0.6–2.7 keV) the model conversion factor is constant within 15%. According to Böhringer et al. (1995) and Böhringer (1999), the temperature of the X-ray emitting intracluster gas in the Virgo cluster is ≈2 keV. In addition to this thermal gas component these authors detected several diffuse emission features near M87 which are significantly softer than the average Virgo cluster gas temperature. However, spectral fits to the ROSAT data do not provide temperatures below 1 keV (Böhringer, private communication). For temperatures near 1 keV the modeled conversion factor for a thermal gas is slightly lower than for higher temperatures. Therefore, the contribution of the lower temperature components to the overall diffuse X-ray emission in the EUV band pass is lower than the dominant 2 keV cluster gas component. Using the conversion factor appropriate for the mean cluster gas temperature of 2 keV for the entire emission including the softer thermal enhancements, slightly overestimates the low energy X-ray contribution to the EUV emission.

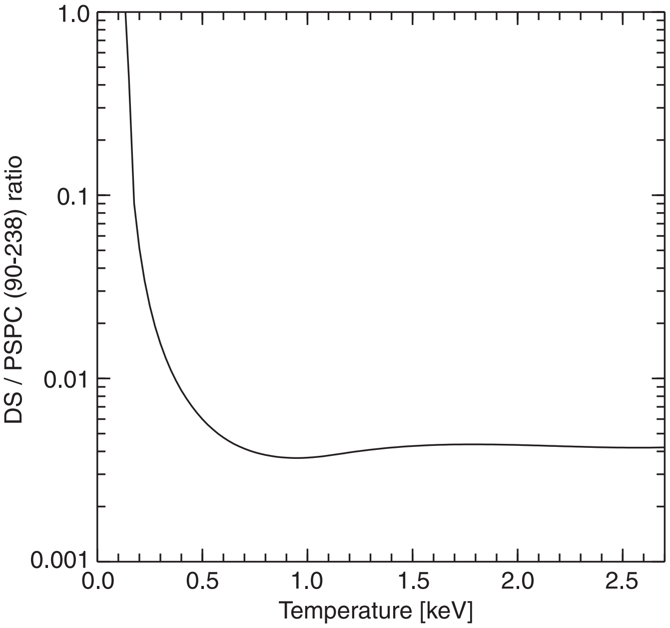

Fig. 3. Modeled conversion factors from ROSAT PSPC count rates into EUVE DS rates for a thermal plasma model including the ISM absorption towards the Virgo cluster.

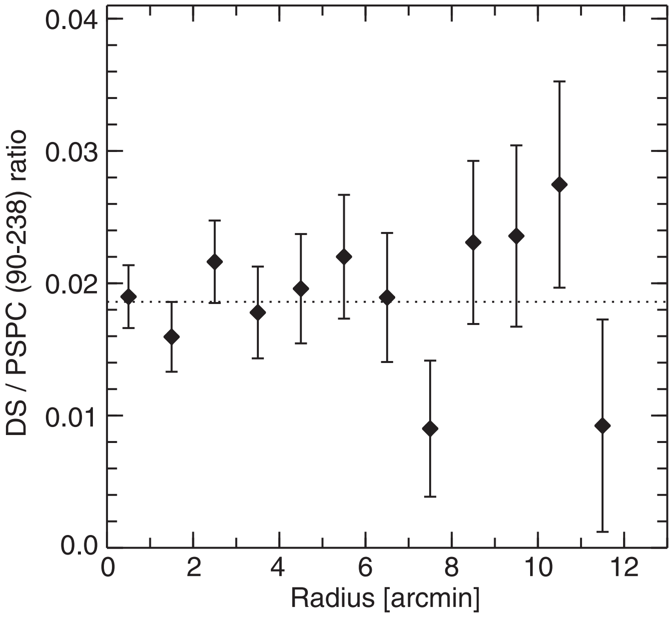

Fig. 4. The ratio between observed azimuthally averaged intensity profiles observed with the EUVE DS and ROSAT PSPC. The dotted line represents the best fit value of 0.186 assuming a constant ratio.

In Figure 4 we show the observed ratio between azimuthally averaged radial intensity profiles observed with the EUVE DS and PSPC. Within the error bars the ratio is constant (reduced $\chi^2 = 0.9$). The best fit value is 0.0186. The ratio for the inner $1'$ bin is consistent with this value, however, we excluded this due to the presence of emission from the core and jet of M87. Sarazin & Lieu (1998) have suggested that an increasing EUV to X-ray emission ratio towards larger distances from the cluster center is an indication of an inverse Compton process producing the EUV emission in the cluster. However, Figure 4 demonstrates that this is not observed in the central Virgo region.

On the other hand, our best fit value of 0.0186 is ≈4.3 times larger than expected for the low energy tail of the X-ray emitting gas in the Virgo cluster. Therefore, the X-ray contribution to the observed EUV excess in the central part of the Virgo cluster must be minor.

It is clear that the ratio between observed EUV flux and modeled X-ray contribution cannot directly be used to determine the physical parameters of the source. Instead, one must first subtract the X-ray contribution from the observed EUV emission.

In Figure 5 we show the spatial distribution of the EUV excess emission in the central Virgo region; the background and the contribution of the low energy tail of the X-ray emitting ICM have been subtracted. The central

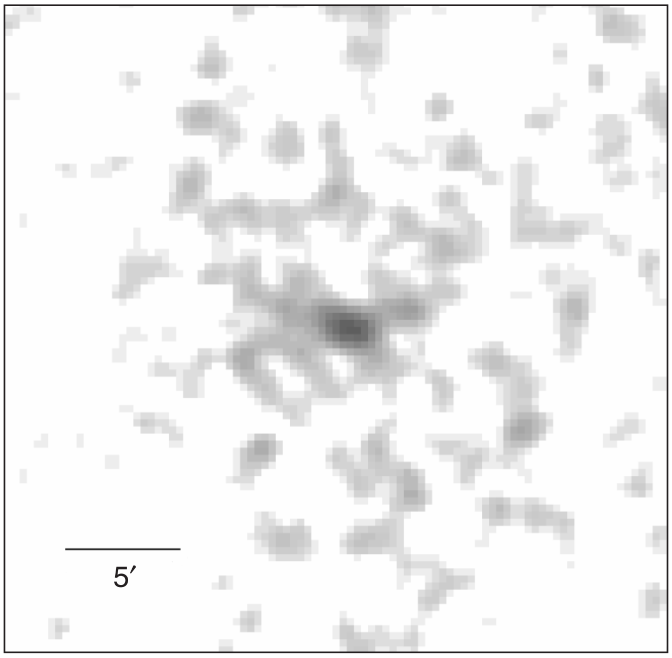

Fig. 5. Spatial distribution of the EUV excess emission in the central Virgo region. The contribution of the low energy tail of the X-ray emitting ICM has been subtracted from the data.

emission peak at the position of M87 is surrounded by a diffuse EUV emission structure which is asymmetric in shape. Its extent varies between 1′and 7′. Several arm-like features are visible. At larger radii the EUV emission results from a number of apparently discrete and extended diffuse features in the M87 radio halo region. These emission features are consistent with the emission seen in the surface brightness profile (Figure 2) between 9–13′. These asymmetric features show the flux is not produced by a gravitationally bound thermal gas.

4. Discussion and Conclusions

The results of our reanalysis show a clear EUV excess in the central Virgo region around M87. Compared to previous studies the extent of this emission is smaller and extends only to ≈13′ from the center of M87.

To further explore the spatial distribution of the EUV excess we compare this emission to a 90 cm radio map of the central Virgo region near M87 (Owen, Eilek & Kassim 1999). If the diffuse EUV emission is due to an inverse Compton process in the ICM one might expect to see similar emission features in both the EUV and radio image. In Figure 6 we show a contour plot of the EUV emission superposed on the 90 cm radio map. As can be seen, the EUV emission peaks at the position of the radio emission of the core and jet of M87. EUV excess emission features are, however not directly coincident with any of the other brighter features visible in the radio map. The EUV emission is also not associated with the X-ray emission features seen in the ROSAT PSPC images in excess of the wide dif-

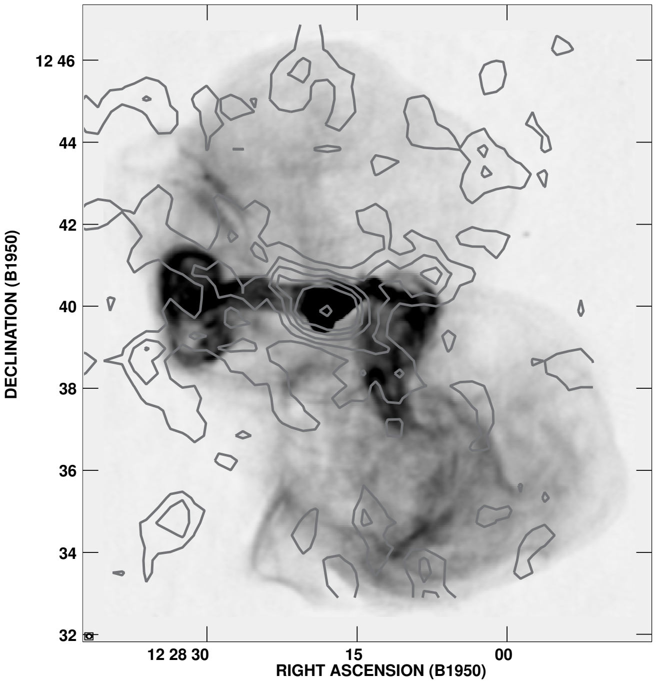

Fig. 6. Contour plot of the background and X-ray subtracted EUV emission shown superposed on the 90 cm radio map of the M87 halo. The contours provide fluxes of 1.5, 4.5, 7, 10, 13, and 27 σ above the noise level.

fuse ICM gas component in Virgo (cf. Böhringer 1999 and Harris 1999).

We now investigate whether the integrated flux of the diffuse EUV emission is compatible with an inverse Compton origin of the observed EUV excess in the central Virgo region. We have used the observed radio synchrotron power law spectrum of the M87 halo ($\alpha = 0.84$, Herbig & Readhead 1992) to compute the underlying distribution of relativistic electrons in this region and its inverse Compton flux. Note that the radio spectrum needs to be extrapolated into the low frequency range near 1 MHz which is not observable due to ionospheric effects. The conversion from the synchrotron spectrum into an electron energy distribution depends on the average magnetic field strength in the ICM and hence we can derive a relation between magnetic field strength and the inverse Compton flux produced by the relativistic electrons. Figure 7 shows the result. The flux is folded with the EUVE DS response and given in units of DS counts/s which allows a direct comparison to the observed integrated DS count rate of the diffuse emission (horizontal line in Figure 7). As can be seen, for a magnetic field strength of $\approx 3\mu$G the observed flux matches the model flux. Note

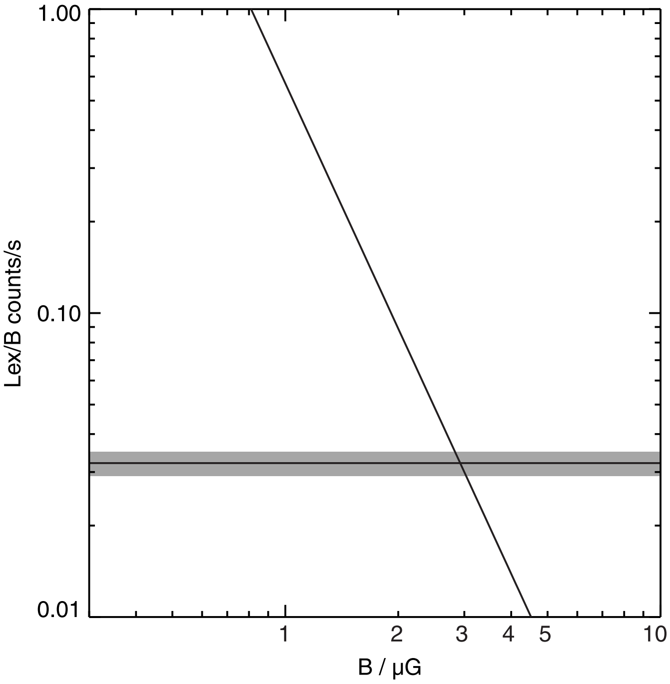

Fig. 7. EUVE DS count rate as a function of magnetic field strength. The horizontal line provides the observed total count rate for the diffuse emission component. The error in this value is shown as a gray shaded area.

that this value would also be consistent with Faraday rotation measurements in the M87 halo (Dennison 1980).

However, with $\alpha = 0.84$ the radio synchrotron spectrum is inconsistent with the required steep EUV to X-ray power law spectrum. In order to explain the observed EUV flux and the upper limit in the ROSAT PSPC hard band (channels 90–238) by a non-thermal power law type spectrum source we find a power law photon number index of $\alpha \geq 3.2$. Therefore, inverse Compton emission from the known population of relativistic electrons in the M87 halo cannot account for the observed EUV excess in the central Virgo region.

5. Summary

The observed EUV excess in the central Virgo region is not spatially consistent with either the distribution of the radio emission or the observed thermal X-ray excess emission seen in the ROSAT images. Due to the required steep EUV to X-ray spectrum this emission cannot be produced by an extrapolation to lower energies of the observed synchrotron radio emitting electrons. Therefore, as is the case in the EUV excess in the Coma cluster (cf. Bowyer & Berghöfer 1998), a second unknown population of relativistic electrons would be required to explain the observed EUV excess by inverse Compton's emission, if this were the underlying source mechanism.

Acknowledgements. We thank Jean Eilek for providing us a postscript file of the M87 radio map. We acknowledge useful discussions with John Vallerga, and Jean Dupuis. This work was supported in part by NASA contract NAS 5-30180. TWB was supported in part by a Feodor-Lynen Fellowship of the Alexander-von-Humboldt-Stiftung. SB and EK have been supported by EUVE.

References

[1] Arabadjis, J. S. & Bregman J. N., 1999, ApJ, 514, 607
[2] Berghöfer, T. W., Bowyer, S., Lieu, R., & Knude, J. 1998, ApJ, 500, 838
[3] Böhringer, H., Nulsen, P. E. J., Braun, R. & Fabian, A. C. 1995, MNRAS, 274, L67
[4] Böhringer, H. 1999, this workshop
[5] Bowyer, S., & Malina, R. F. 1991, in Extreme Ultraviolet Astronomy, ed. R. F. Malina & S. Bowyer (New York: Pergamon), 397
[6] Bowyer,S., & Berghöfer, T. W. 1998, ApJ, 506, 502
[7] Bowyer,S., Berghöfer, T. W. & Korpela, E. 1999, this workshop
[8] Dennison, B. 1980, ApJ, 236, 761
[9] Harris, D. 1999, this workshop
[10] Hartmann, D., & Burton, W. B. 1997, Atlas of Galactic Neutral Hydrogen (Cambridge: Cambridge Univ. Press)
[11] Herbig, T., & Readhead, A. C. S. 1992, ApJS 81, 83
[12] Hwang, U., Mushotzky, R. F., Loewenstein, M., Markert, T. H., Fukazawa, Y. & Matsumoto, H. 1997, ApJ, 476, 560
[13] Lieu, R., Mittaz, J., Bowyer ,S., et al. 1996, ApJl, 458, L5
[14] Owen, F., Eilek, J. & Kassim, N., 1999, in prep.
[15] Sarazin, C., & Lieu, R. l998, ApJ, 494, L177

Proceedings of the Workshop: *"Diffuse Thermal and Relativistic Plasma in Galaxy Clusters"*
Ringberg Castle, Germany, April 19–23, 1999, eds. H. Böhringer, L. Feretti & P. Schuecker, MPE Report 271, pp. 212-218

On the Broad Band Nonthermal Emission of Galaxy Clusters

Armen M. Atoyan[1,2] **and Heinz J. Völk**[1]

[1] Max–Planck–Institut für Kernphysik, Postfach 103980 , D-69029 Heidelberg, Germany
[2] Yerevan Physics Institute, Alikhanian Broth. 2, 375036 Yerevan, Armenia

Abstract. The inverse Compton (IC) interpretation of the excess EUV emission detected recently from several clusters of galaxies suggests a very significant amount of relativistic electrons in the intracluster medium. Considering Coma as the prototype galaxy cluster of nonthermal radiation, with the nonthermal fluxes measured from radio frequencies to (possibly) the X-ray region, we discuss implications of the inverse Compton origin of the EUV fluxes in the case of low magnetic fields of order $0.1\,\mu$G as required for the IC interpretation of the observed excess X-ray flux, and in the case of high magnetic fields of order $1\,\mu$G as suggested by the radio observations. In particular we show that for the high intracluster field the excess EUV flux can be explained by the IC emission of the relic population of electrons driven into the incipient intracluster medium at the epoch of starburst activity by the galactic winds which presumably are at the same time responsible for the comparatively strong magnetic fields in clusters of galaxies. Radiative cooling would produce a sharp cutoff in the spectrum of these 'relic' electron population, which is necessary in the case of μ-Gauss fields in order to avoid a contradiction with the observed radio fluxes. The radio fluxes of Coma would then require a second component of electrons to be injected recently, and could be produced in particular as secondaries by a reasonable amount of relativistic protons. We calculate the fluxes of γ-rays to be expected in, both, the low and high magnetic field scenarios, and discuss possibilities to distinguish between these two principal options by future γ-ray observations.

1. Introduction

One of the significant characteristics of galaxy clusters is their nonthermal particle content. An unambiguous signature of the presence of relativistic electrons, and by implication also of relativistic protons, in the intracluster medium (hereafter ICM) is the detection of a diffuse cluster-scale radio emission from a number of these objects (see e.g. Giovannini et al. 1999, and references therein). The radio fluxes give an important information on the energy spectra of the electrons in the ICM, but being dependent on the ICM magnetic fields, they do not yet allow unambiguous estimates of the overall energy content of relativistic electrons. More accurate estimates can be derived if one interprets the 'excess' diffuse EUV emission reported from some clusters (e.g. Lieu et al. 1996, Mittaz et al. 1997, Bowyer et al. 1997) in terms of inverse Compton (IC) upscattering of 2.7 K microwave background radiation by electrons with energies of a few 100 MeV (e.g. Hwang 1997, Sarazin & Lieu 1998, Enßlin & Biermann 1998). This typically requires an overall energy in these electrons of order 10^{61} erg. Depending on the spectra of relativistic electrons at lower energies, and on the ratio of the relativistic protons to electrons, the total energy in cosmic rays (CRs) might be then as high as $W_{\rm CR} \sim (10^{62} - 10^{63})$ erg.

Thus, CRs may contain a significant fraction of the overall kinetic energy in the ICM and could be dynamically important. Because the energy loss time of CR particles in the ICM typically exceeds the Hubble time, and since their confinement time generally exceeds the cluster lifetime (Völk et al. 1996, Berezinsky et al. 1997, Colafrancesco & Blasi 1998), the nonthermal component of galaxy clusters should contain valuable information about the evolution of these largest gravitationally bound systems of the Universe.

In this paper we will study in detail the broad band nonthermal emission of the Coma cluster which is considered as a prototype nonthermally emitting cluster, with nonthermal radiation fluxes reported both in the radio and the EUV regions. Until now the Coma cluster remains the only cluster where the 'excess' emission is firmly established also in the region of hard X-rays (Fusco-Femiano et al. 1999; Rephaeli et al. 1999). Interpretation of this emission in terms of IC radiation of electrons, responsible also for the radio fluxes at low frequencies, suggests that the ICM magnetic field in Coma is about $0.1 - 0.2\,\mu$G. In section 2 below we consider the IC interpretation of the excess X-ray flux, and calculate the fluxes of IC radiation to be expected in the γ-ray region. It is quite possible however that the ICM magnetic field in Coma is at the level of $\geq 1\,\mu$G, as deduced from Faraday rotation and depolarization measurements on background radio sources (Kim et al. 1990, Feretti et al. 1995). Although an IC origin of the excess X-ray flux in that case is excluded, we show in section 3 that an IC origin of the excess EUV flux is still possible. We demonstrate that a rather unusual energy distribution of the relativistic electrons (needed to comply with the data both in EUV and the radio region) can be naturally formed during the cosmological evolution of Coma. In particular, these electrons could be the relics of the early starburst activity in the Coma galaxies which fed the incipient ICM with relativistic particles and magnetic fields via their galactic winds (Völk & Atoyan 1999). In section 4 we calculate the γ-ray fluxes to be expected in the case of high magnetic field and discuss whether it would be possible to distinguish between high and low magnetic field scenarios by future γ-ray detectors.

2. IC Interpretation of the Excess X-Rays

Radio fluxes from the Coma cluster are detected from 10.3 MHz to 2.7 GHz (Bridle and Purton, 1968; Henning 1989; Kim et al. 1990; Giovannini et al. 1993), and at 4.85 GHz an upper flux limit was reported by Kim et al. (1990). The differential energy fluxes $J_\nu \propto \nu^{-\alpha_{\rm r}}$ between 30.9 MHz and 1.4 GHz are well fitted with a power-law index $\alpha_{\rm r} = 1.16$. The data at 2.7 and 4.85 GHz fall below this extrapolation, so that the 'best fit' single power-law index would then correspond to $\alpha_{\rm r} = 1.36$ (Schlickeiser et al. 1987). Note however that the reported sharp decline of the radio fluxes above 1.4 GHz can also be explained as an instrumental effect (Deiss 1997).

The diffuse excess (over the thermal) radiation between 65 eV and $\simeq$ 200 eV has a mean power-law index $\alpha_{\rm euv} \sim 0.75$ (Lieu et al. 1999). The power-law index of the diffuse excess X-rays is rather uncertain and lies most probably within the range of $\alpha_{\rm x} \simeq (1-2)$ (see Fusco-Femiano et al. 1999, Rephaeli et al. 1999). This range includes the values of the spectral indices $\alpha_{\rm r}$ of the radio fluxes, which in principle allows an interpretation of the X-ray flux in terms of IC radiation of the same population of electrons which are responsible for the synchrotron emission at radio frequencies.

The characteristic frequency of synchrotron radiation of electrons with Lorentz factor γ is $\nu \simeq B_{\mu\rm G}\,\gamma^2$ Hz where $B_{\mu\rm G} \equiv B/1\,\mu$G (e.g. Ginzburg 1979). Thus the production of synchrotron radiation in the region from 10 MHz to 1.4 GHz requires that the energy distribution of the electrons $N(\gamma) \propto \gamma^{-\alpha_{\rm e}}$ extends with an index $\alpha_{\rm e} = 1 + 2\alpha_{\rm r} \approx (3.2-3.6)$ from $\gamma_{\rm r,1} \simeq 3\times10^3\, B_{\mu\rm G}^{-0.5}$ to $\gamma_{\rm r,2} \simeq 4\times10^4\, B_{\mu\rm G}^{-0.5}$.

For the IC process the mean energy of photons produced in the 2.7 K background radiation field with the mean photon energy $\epsilon_0 \simeq 3\,kT$ is $\epsilon \simeq (4/3)\epsilon_0\,\gamma^2 \simeq 8.7\times10^{-4}\,\gamma^2$ eV. For the production of the X-ray photons from 20 keV to 80 keV one therefore needs electrons with energies between $\gamma_{\rm x,1} \simeq 5\times10^3$ and $\gamma_{\rm x,2} \simeq 10^4$. Because the latter actually corresponds to the lower edge $\gamma_{\rm r,1}$ of the electrons responsible for the observed radio emission (in magnetic fields of order $0.1\,\mu$G), the spectral index of the X-ray emitting electrons should be close to $\alpha_{\rm e}$ as derived from radio data.

The IC origin of Coma's EUV spectrum from 70 eV to 200 eV implies a spectral index $\alpha_{\rm e} \sim 2.5$ for the electrons in a rather narrow energy region around $\gamma_{\rm euv} \simeq 300$. A gap by a factor of ≥ 10 between $\gamma_{\rm euv}$ and $\gamma_{\rm r,1}$ allows then a scenario with a single population of power-law electrons where radiative losses induce a break in $\alpha_{\rm e}$ somewhere in that gap. Thus assuming a source function of electrons $Q(\gamma) \propto \gamma^{-\alpha_{\rm inj}}$ in the ICM with $\alpha_{\rm inj} = 2.3$, the IC emission of those electrons at low energies will give $\alpha_{\rm euv} = 0.65$, which is acceptably close to the value 0.75. After the break, the electron distribution steepens to $\alpha_{\rm e} = 1 + \alpha_{\rm inj} = 3.3$ required for interpretation of the radio fluxes.

Such a break in the energy spectrum can be produced by radiative losses of electrons if they are injected into the ICM on time scales $\Delta t_{\rm inj} \geq 10^9$ yr. For the energy loss rate due to IC (in the Thompson limit) and synchrotron processes

$$P(\gamma) = -\frac{{\rm d}\gamma}{{\rm d}t} = \frac{4\,\sigma_{\rm T}}{3\,m_{\rm e}c}\left(w_{\rm mbr} + \frac{B^2}{8\pi}\right)\gamma^2 \;, \qquad (1)$$

the characteristic energy loss time is

$$t_{\rm rad} \approx 2.4\times10^{12}[(1+z)^4 + 0.1B_{\mu\rm G}^2]^{-1}\,\gamma^{-1}\ {\rm yr}\;, \qquad (2)$$

where we take into account the cosmological evolution of the energy density of the cosmic microwave background radiation $w_{\rm mbr} \propto (1+z)^4$ at the epoch z. For magnetic fields $B < 3\,\mu$G the radiative losses are dominated by the IC process. Using Eq. (2), from the condition $t_{\rm rad}(\gamma) \simeq \Delta t_{\rm inj}$ we find that the radiative break would appear in the 'proper' place ($\gamma_{\rm br} \sim 10^3$) if relativistic electrons were injected into the ICM recently, during times $t_{\rm inj} \sim (1-3)\times10^9$ yr (this corresponds to $z_{\rm inj} \leq 0.2$). Note that the relativistic electrons need to be produced/accelerated in the ICM *continuously* during that time period, because in the case of an 'impulsive' injection the radiative losses induce a cutoff, and not a break, above $\gamma_{\rm br}$.

In Fig. 1 we show the results of calculations when the same $B = 0.12\,\mu$G and $\Delta t_{\rm inj} = 3$ Gyr are assumed for 3 different power-law indices $\alpha_{\rm inj}$ of the electron injection spectrum

$$Q(\gamma) \propto \gamma^{-\alpha_{\rm inj}}\exp(-\gamma/\gamma_{\rm c}), \qquad (3)$$

where $\gamma_{\rm c}$ defines the characteristic maximum energy of the accelerated particles. The synchrotron fluxes are normalized to the radio flux from the Coma cluster observed at 400 MHz. For the assumed magnetic field, the IC 'counterpart' of this normalization point in Fig. 1 is found at the photon energy $\epsilon \approx 1$ MeV, and therefore for different indices $\alpha_{\rm inj}$ the IC fluxes predicted in the X-ray region are somewhat different. Because the synchrotron flux at a given frequency depends on the overall number of radio electrons and magnetic field as $L_{\rm syn} \propto N_{\rm e}B^{(1+\alpha_{\rm e})/2}$,

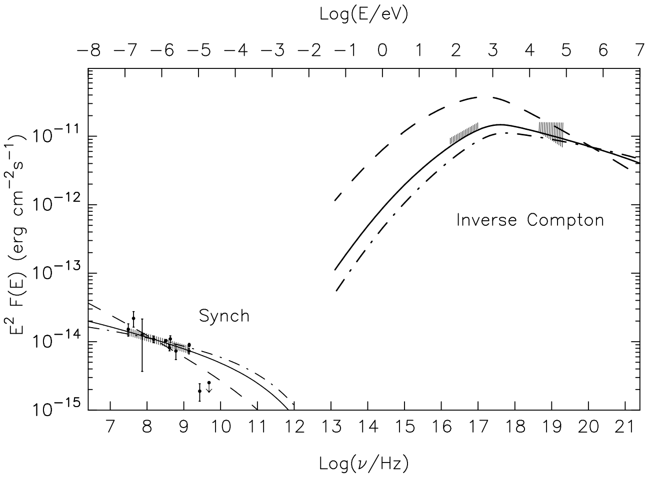

Fig. 1. The synchrotron and IC fluxes calculated for the magnetic field in Coma cluster $B = 0.12\,\mu$G, assuming stationary injection of relativistic electrons during the last $\Delta t_{\rm inj} = 3\times 10^9$ yr, and 3 different power-law indices for the source function $Q(\gamma)$ in Eq.(3): $\alpha_{\rm inj} = 2.2$ (dot-dashed curves), $\alpha_{\rm inj} = 2.3$ (solid), and $\alpha_{\rm inj} = 2.6$ (dashed). An exponential cutoff energy $\gamma_{\rm c} = 2\times 10^6$ is assumed. The source function is chosen so that the radio spectrum is normalized to the observed flux at 400 MHz. The compilation of radio data and the slope of the hatched region from 30 MHz up to 1.4 GHz, corresponding to a power-law index $\alpha_{\rm r} = 1.16$ for the differential energy flux $J(E) = EF(E)$, are taken from Deiss et al (1997). The hatched regions in the EUV and X-ray domains correspond to the fluxes observed by Lieu et al (1999), and Rephaeli et al (1999) and Fusco-Femiano et al (1999), respectively.

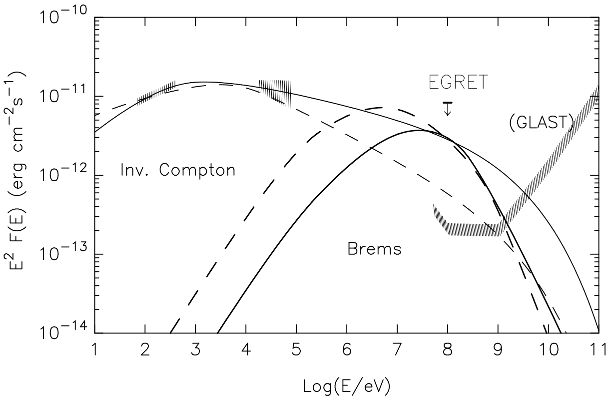

Fig. 2. The bremsstrahlung and IC radiation fluxes calculated in the case of injection of relativistic electrons with $\alpha_{\rm inj} = 2.3$ during the last $\Delta t_{\rm inj} = 3$ Gyr assuming $B = 0.1\,\mu$G (solid curves), and $\alpha_{\rm inj} = 2.6$, $\Delta t_{\rm inj} = 1$ Gyr assuming $B = 0.15\,\mu$G (dashed curves). A mean gas density $n_{\rm g} = 10^{-3}\,{\rm cm}^{-3}$ in the ICM is assumed. In the γ-ray region, the expected flux sensitivity of the GLAST detector (from Bloom 1996) and the upper flux limit of EGRET (Sreekumar et al 1996) are also shown.

the X-ray fluxes can be increased or decreased assuming slightly lower or higher magnetic fields. Thus for the injection spectrum with $\alpha_{\rm inj} = 2.2$ a field somewhat smaller than the $B \approx 0.12\,\mu$G assumed in Fig. 1 would be needed to explain the observed fluxes both in the EUV and in the X-ray regions. In the case of a steep spectrum with $\alpha_{\rm inj} = 2.6$ an increase of the field to $B \approx 0.15\,\mu$G could reduce the IC flux to within the range of the observed 'excess' fluxes in the X-ray region. But, in addition, we have to assume a more recent time for the injection of relativistic electrons in the ICM – in order to induce the radiative break at higher energies and to explain also the excess EUV flux.

Thus, uncertainties in the reported fluxes and spectral indices of the radiation in different energy bands allow some latitude in the predictions of the magnetic field in the Coma cluster. In Fig. 2 we show the spectra of IC radiation calculated for two different sets of the parameters B, $\alpha_{\rm inj}$, and $\Delta t_{\rm inj}$. Note that the value of $B \approx 0.15\,\mu$G needed in the case of a steep radio spectrum with $\alpha_{\rm r} = 1.3$ (i.e. $\alpha_{\rm inj} = 2.6$) agrees well with the magnetic field deduced by Fusco-Femiano et al. (1999) from comparison of the radio fluxes with the excess X-ray flux detected by the BeppoSAX detector. A further increase of the magnetic field, up to $B \leq 0.2\,\mu$G (Rephaeli et al. 1999), would be possible only for a smaller flux of the IC X-rays.

The total energy in relativistic electrons which is needed for the interpretation of the excess EUV and X-ray fluxes in Fig. 3 is equal to $W_{\rm e} = 6.3\times 10^{61}$erg and $W_{\rm e} = 1.8\times 10^{62}$erg for $\alpha_{\rm inj} = 2.3$ and $\alpha_{\rm inj} = 2.6$, respectively. For such a high total energy of relativistic electrons, with the spectra extending beyond 100 GeV energy (needed for the interpretation of the radio fluxes), the fluxes of IC gamma-rays should extend to the region of high energy γ-rays. In the case of power-law spectra in the radio region with $\alpha_{\rm r} \simeq (1.1-1.2)$, the extension of the IC fluxes with the same index from the X-ray to the γ-ray region predicts fluxes observable for the future GLAST detector (see solid line in Fig. 2). For steep spectra with $\alpha_{\rm r} \geq 1.3$, the predicted IC flux would be only marginally observable. However, because of the high gas density in the Coma cluster (up to $3\times 10^{-3}\,{\rm cm}^{-3}$ in its centre, Briel et al. 1992) the flux of bremsstrahlung γ-rays should be observed by GLAST in any case (see Fig. 2).

3. IC Origin of the EUV Flux in High Magnetic Fields

The conclusion that the magnetic field in Coma cluster is small, $B \sim (0.1-0.2)\,\mu$G, is an unavoidable result of the assumption that the observed excess X-ray flux has an inverse Compton origin. However, the values of the magnetic field in Coma (Kim et al 1990, Feretti et al 1995), deduced from radio observations are at a level of $B \geq 1\,\mu$G, which is also typical for other clusters (Kronberg 1994).

If this is the case, then an IC origin of the excess hard X-rays in Coma is absolutely excluded. Indeed, the target photon field for such IC radiation is well known. Therefore the total number of electrons $N_e(\gamma)$ in the energy range $\gamma \sim 5\times10^3-10^4$ is fixed. Because these energies are larger than $\gamma_{r,1} \simeq 3\times10^3 B_{\mu G}^{-0.5}$ for fields of the order of $1\,\mu$G (see section 2), the synchrotron radiation of those 'IC X-ray' electrons would be at frequencies $\nu > 10\,$MHz, accessible for radio observations. An increase of the magnetic field by one order of magnitude compared with what is assumed in Fig. 1 would thus result in overproduction of the radio fluxes at least by two orders of magnitude.

However, for the excess EUV flux an IC origin can still not be excluded if in the energy region from $\gamma_{euv} \sim 300$ to $\gamma_{r,1}$ the energy distribution of the electrons would decline extremely fast, even as compared with the standard power-law $N(\gamma)$ with $\alpha_e \geq 3$, in order to reduce by those two orders of magnitude the total number of the electrons with $\gamma \geq \gamma_{r,1}$. Basically, this implies a sharp cutoff in $N(\gamma)$ somewhere in the gap between γ_{euv} and $\gamma_{r,1}$. This scenario then suggests that the populations of relativistic electrons with energies below a few 100 MeV, responsible for the EUV emission, should be different from the population of electrons of higher energies producing the radio emission in Coma.

Here we suggest that the low energy electrons can be naturally connected with the old population of relativistic electrons injected into the incipient ICM early on at the epoch of the initial starburst activity in the Coma galaxies. Powerful galactic winds, the past existence of which appears to be necessitated by the observed high iron abundance, could enrich the ICM also with relativistic particles and magnetic fields (Völk et al 1996; Völk & Atoyan 1999). Then a sharp radiative cutoff – instead of a radiative break – below $\gamma_{r,1}$ will be naturally produced in the spectrum of the relativistic electrons injected early on into the ICM, provided that the injection/acceleration of these electrons has stopped, or at least has sharply declined, at some epochs $z > 0.05$ (corresponding to the last $\Delta t > 10^9\,$yr).

Assuming for convenience of calculations the Einstein-de Sitter Universe ($\Omega_0 = 1$), the cosmological time is

$$t(z) = \frac{2}{3H_0(1+z)^{3/2}} = 1.3\times10^{10}(1+z)^{-3/2}\,\mathrm{yr}\,, \quad (4)$$

chosing $H_0 = 50\,$(km/s)/Mpc for the Hubble constant. Integrating then Eq.(1) over time, one easily finds that all electrons which have been injected into the ICM at an epoch $z > 0$ would at present be cooled down, due to IC losses, to energies below

$$\gamma_{cut} = \frac{310}{(1+z)^{5/2}-1}\,. \quad (5)$$

If these electrons were not reaccelerated at some $z' < z$, their energy distribution should have a sharp cutoff at $\gamma = \gamma_{cut}(z)$. Note that for $z \sim 1$ or larger, $\gamma_{cut} \propto (1+z)^{-5/2}$. This dependence readily follows from the comparison of Eqs.(1) and (4), which indicates that most of the radiative cooling of the electrons, and thus the formation of the cutoff in the energy spectrum, occurs at the early epoch as the injection/acceleration of relativistic electrons in the ICM drops.

For the further calculations we approximate the injection spectrum of electrons by a power-law energy distribution cf. Eq.(3), and with a time profile for the injection rate in the form

$$q(t) = \begin{cases} 1 & ,\ t(z_0) \leq t \leq t(z_1) \\ [t(z_1)/t]^m & ,\ t(z_1) \leq t \leq t(0) \end{cases} \quad (6)$$

Here the epochs z_0 and z_1 correspond to the beginning and to the end of an efficient injection of relativistic electrons into the ICM, so that the difference $\Delta t_{inj} = t(z_1) - t(z_0)$ has the meaning of a characteristic duration of the electron injection phase ('starburst activity'). Lack of space forces us to give the details of calculations of the electron energy distribution elsewhere (Atoyan & Völk 1999). Here we only note that we take the cosmological evolution of the cosmic microwave background radiation into account, and that along with the radiative losses we also consider possible Coulomb ('ionization') and bremsstrahlung losses of electrons in the ICM.

The electron energy distributions calculated for $q(t)$ declining with different indices m are shown in Fig. 3. A stationary injection during $\Delta t_{inj} = 2\,$Gyr starting from $t(z_0 = 1.5) \approx 3.3\,$Gyr is assumed. This results in the epoch $z_1 \approx 0.8$ when the injection rate starts to decline. A significant cutoff or a 'knee' in the electron distribution above $\gamma_{cut}(0.8) = 93$ is formed only if the injection rate drops sharply, $m \geq 4$. Otherwise the electron injection currently remains high enough in order to fill up the knee with recently accelerated electrons, resulting in a feature resembling more an ordinary spectral break rather than a cutoff at $\gamma \sim \gamma_{cut}(z_1)$. Such an extraordinary fast decline of $q(t)$ would actually mimic a Gaussian type function, with a dispersion $\sigma_t \simeq \Delta t_{inj}/2$ significantly smaller than the time interval $t(0) - t(z_{sb})$ between the epoch z_{sb} of the maximum injection rate and the present time $t(0)$. Note that this kind of injection could be a quite appropriate approximation for the electrons injected into the incipient ICM at the epoch of early starburst activity.

The absolute values of the fluxes in Fig.4 could be changed assuming a different total energy for the injected electrons. However the cutoff in the IC radiation would remain below the EUV region. Formally, the cutoff in the energy distribution of the electrons could be shifted to values $\gamma_{cut} \geq 500$ needed for an explanation the EUV flux, if we would assume that the phase of active injection of the electrons were continued until very recent epochs, $0.05 \leq z_1 \leq 0.2$, but then it just stopped. However, this kind of assumption could hardly find any physical justification, especially if this population of electrons is due to the early starburst activity in Coma.

Much more realistic seems to be a scenario where relativistic electrons driven into ICM by the galactic winds at

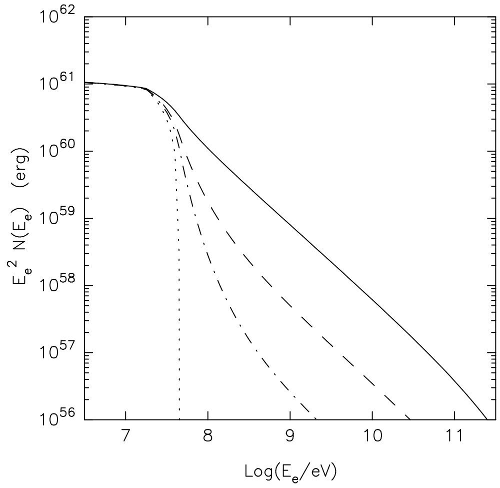

Fig. 3. The energy spectrum of electrons injected at the epoch $z = 1.5$, calculated assuming an injection spectrum with $\alpha_{\rm inj} = 2.1$ with a time profile of the injection, Eq.(6), described by $\Delta t_{\rm inj} = 2\,{\rm Gyr}$, but for different decline rates: $m = 2$ (solid), $m = 4$ (dashed), $m = 6$ (dot-dashed), and $m = \infty$ (dotted curve). In all cases the overall injected energy is $W_{\rm e} = 10^{61}$ erg. It is assumed also that the gas density in the ICM at early epochs was $n_{\rm g} < 10^{-4}\,{\rm cm}^{-3}$

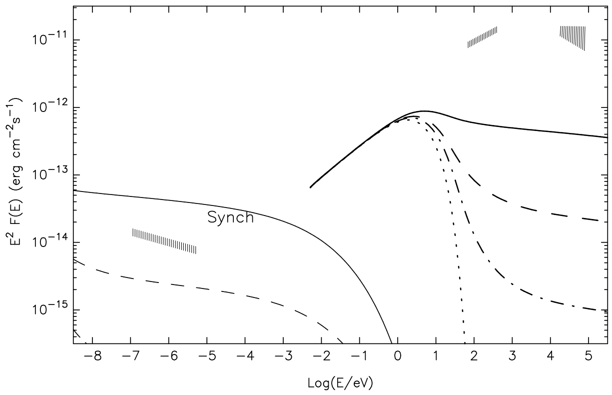

Fig. 4. The fluxes of synchrotron and IC radiations produced by electrons shown in Fig.3. A mean magnetic field $B = 1\,\mu$G in the cluster is supposed.

the times of the early starburst activity at $z_{\rm sb} \geq z_1 \sim 1$, had cooled down to energies $\gamma_{\rm cut}(z_1) < 100$, however remaining relativistic. Then, the passage of even a single strong shock across the cluster, e.g. due to a galaxy merger, would be sufficient to reaccelerate these electrons to GeV and higher energies. In the downstream region after the passage of the shock the electrons would again be radiatively cooled down. A cutoff in the energy spectrum of the electrons will then appear at energies $\gamma \geq 500$ if such a shock(s) occurred at $z \leq 0.2$ (i.e. during the recent $\Delta t \leq 3\,{\rm Gyr}$).

Another interesting possibility is connected with a purely adiabatic energization of that relic population of electrons by compression of the ICM gas due to contraction of the cluster. An interesting feature of the adiabatic compression is that it does not change the shape of the initial energy distribution of the electrons, but just moves their energy by a factor of a: $N(\gamma) = N_0(\gamma/a)/a$. Therefore, after this kind of energization, the cutoff in the energy distribution of the relic population would be conserved, and there is no need to assume that the compression has stopped some $\Delta t \geq 10^9$ yr ago (in order to allow the formation of the cutoff due to radiative losses). For relativistic particles the parameter $a = (n/n_0)^{1/3}$, where n_0 and n are the ICM gas densities before and after compression. Assuming that the electron injection connected with the starburst activity in cluster galaxies was basically over at say $z \simeq 1$, for the spectral cutoff formed at that epoch we would have $\gamma_{\rm cut} \sim (60-70)$. Pushing this cutoff up by a factor of $a \simeq 10$, we could explain the observed excess EUV flux of Coma by IC radiation of the reenergized relic 'starburst' population of electrons, but without overproduction of the radio fluxes at frequencies $\nu > 10\,{\rm MHz}$ in a high ICM magnetic field $B = 1\,\mu$G (see Fig.5).

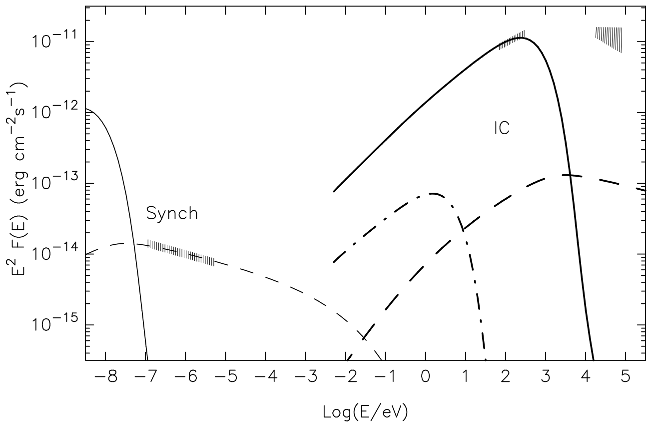

Fig. 5. The fluxes of synchrotron and IC radiations produced by the relic population of electrons injected into the ICM between the epochs $z_0 = 1.5$ and $z_1 = 1$, and later on compressed by a factor $a = (n/n_0)^{1/3} = 11$ (solid lines). The spectrum of IC radiation of the electrons before adiabatic compression is shown by the dot-dashed line. The total injected energy of the electrons $W_{\rm e}^{\rm (inj)} = 1.2 \times 10^{61}$ erg, and $\alpha_{\rm inj} = 2.1$. For the assumed magnetic field $B = 1\,\mu$G, the observed radio fluxes require a second population of electrons, e.g. assuming an injection with $L_{\rm inj} = 2.9 \times 10^{43}\,{\rm erg/s}$, during the recent $\Delta t = 1.7\,{\rm Gyrs}$ (dashed curves).

An adiabatic energy amplification factor $a \sim 10$ implies an increase of the gas density by a factor $\sim 10^3$. In principle, a compression to even significantly larger factors is possible in the cooling flows of galaxy clusters. And although Coma appears to be a cluster without such a flow, compression of the gas up to 3 orders of magnitude in its central region might be also possible. Note that the angular size of the excess EUV emission region (Bowyer & Berghöfer 1998) correlates well with the radius of the central core $\theta_{\rm c} \simeq 10'$ of the (thermal) X-ray emission region (Briel et al. 1992), where the maximum gas density is as high as $\approx 3 \times 10^{-3}\,\mathrm{cm}^{-3}$, and the mean gas density in the entire EUV emission region can be reasonably estimated as $n \simeq 10^{-3}\,\mathrm{cm}^{-3}$. Thus, the parameter a can be about 10 if the gas density profile in Coma started its formation (due to contraction, galaxy mergers) from $n_0 \simeq 10^{-6}\,\mathrm{cm}^{-3}$ [1]. This would then imply that the ICM gas in the core of the Coma has been increased to the level of $10^{-3}\,\mathrm{cm}^{-3}$ not earlier than during the last several Gyrs, because otherwise this initial value of n_0 were smaller than the primordial baryonic density. It is important to note also that only a moderate degree of the gas compression (i.e. a smaller a) will be needed if we combine this adiabatic compression scenario with merger shock reacceleration at some $z' < 1$.

The interpretation of the radio fluxes from the Coma cluster in the case of high magnetic fields requires a second component of relativistic electrons injected into the ICM at more recent times $\Delta t \leq 10^9\,\mathrm{yr}$. Because the overall number of such electrons needed for production of the observed radio fluxes is relatively small, the observed excess X-ray flux cannot be produced by those electrons (see dashed curves in Fig.5), and some other interpretation (e.g. contribution of a high-temperature plasma?) has to be considered. At the same time, magnetic fields $B \geq 1\,\mu\mathrm{G}$ allow a scenario where this second component of the electrons in Coma is due to cosmic ray protons and nuclei interacting with the gas (via production and decay of $\pi^{\pm}$-mesons, $pp \to \pi^{\pm} \to \mu^{\pm} \to e^{\pm}$). Thus, the injection rate of radio electrons assumed in Fig.5 could be provided by relativistic protons with total energy $W_{\mathrm{CR}} \leq 3 \times 10^{62}\,\mathrm{erg}$ (depending on the CR spectrum at energies $E_{\mathrm{p}} < 100\,\mathrm{GeV}$). This seems to be a quite reasonable value, which can be compared with the energy $W_{\mathrm{e}} \simeq 10^{61}\,\mathrm{erg}$ assumed to be injected into Coma in relativistic electrons initially (via galactic winds), and with the energy $W_{\mathrm{e}} = 4.8 \times 10^{61}\,\mathrm{erg}$ in the 'relic' electrons presently – i.e. after their compression and/or reacceleration. It might also be meaningful that the Coma cluster is characterized with a very high mean gas density up to Mpc spatial scales, comparable with the scales of the observed radio emission.

4. Gamma-Ray Emission.

An inverse Compton origin of the excess EUV emission requires an overall energy in relativistic electrons with $\gamma \sim 300$ of order $5 \times 10^{60}\,\mathrm{erg}$ in order to produce the observed flux. Given a high gas density in Coma, the expected fluxes of the bremsstrahlung γ-rays should be significant in both scenarios assuming low or high magnetic fields. The solid curve in Fig.6 shows the fluxes of bremsstrahlung γ-rays produced by the 'relic' population of the electrons which explain the EUV flux of Coma in Fig.5.

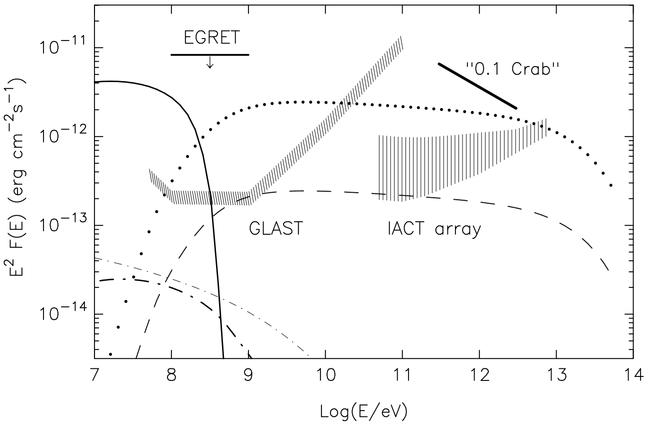

Fig. 6. γ-ray fluxes expected from the Coma cluster. The solid curve shows the bremsstrahlung flux produced by the 'relic' population of electrons which explains the observed EUV flux of Coma in Fig.5. Heavy dot-dashed and thin dot-dashed curves show the bremsstrahlung and IC fluxes produced by the radio electrons (in the case of $B = 1\,\mu\mathrm{G}$). Dotted and dashed curves correspond to the fluxes of π^0-decay γ-rays produced by CR protons with total energy $W_{\mathrm{CR}} = 3 \times 10^{62}$ and 3×10^{61} erg, respectively (for $\alpha_{\mathrm{pr}} = 2.1$). The lower and upper edges of the shown range of sensitivities of IACT arrays correspond to a point source and an extended ($\Delta\theta = 1^{\circ}$) source, respectively (see Aharonian et al. 1997). For comparison, the flux level corresponding to 10% of the Crab Nebula flux (e.g. Konopelko et al. 1998) is also shown.

A remarkable feature of the bremsstrahlung spectrum in Fig.6 is the very sharp cutoff at energies above a few 100 MeV. Comparison of this spectrum with the γ-ray fluxes shown in Fig.2 reveals that the scenario assuming low magnetic field in Coma, $B \sim 0.15\,\mu\mathrm{G}$, can be easily distinguished from the case of high magnetic field by an essentially more gradual decline (if any at all) of γ-ray fluxes above 300 MeV produced by GeV and higher energy electrons (for the IC origin of the X-rays) due to both the bremsstrahlung and the IC processes. An IC origin of the EUV emission of Coma predicts in both cases γ-ray fluxes well above the level of sensitivity of the future GLAST detector which thus would help to resolve the problem of low *vs.* high magnetic field in Coma. This possibility to probe the strength of the magnetic field could be available also for other clusters with excess EUV emission if their gas density would be high.

Thus, the detection of a sharp cutoff in the spectrum of high energy γ-rays by GLAST would confirm the $\geq 1\,\mu\mathrm{G}$ level of the magnetic field in Coma. We note however that an absence of such a cutoff will not yet mean that the magnetic field is low. At energies above 100 MeV one can expect also significant fluxes of γ-rays due to the production and the decay of π^0-mesons if the energy content in relativistic protons in the central $\leq 1\,\mathrm{Mpc}$ region of Coma is high, with $W_{\mathrm{CR}} \geq 10^{62}\,\mathrm{erg}$. Fig.6 shows that the total energy flux of the bremsstrahlung (solid curve) and π^0-decay (dotted curve) γ-rays may have even a sin-

[1] Note that even presently the inferred density of the thermal gas at radii $\theta \simeq 100'$ (corresponding to $r \simeq 4\,\mathrm{Mpc}$) is $\sim 10^{-5}\,\mathrm{cm}^{-3}$ (see Briel et al. 1992)

gle power-law form if $W_{\rm CR} \sim 3 \times 10^{62}$ erg. On the other hand, Fig.6 shows also that in that case the fluxes of π^0-decay γ-rays should be detectable also by the forthcoming imaging atmospheric Cherenkov telescope (IACT) arrays in the region of very high energies, $E \geq 100\,$GeV. Note that the upper edge of the range of expected sensitivities of such IACT arrays (Aharonian et al. 1997), shown in Fig.6, corresponds to an extended source with angular size $\Delta\theta \simeq 1°$, and the lower edge is for a 'point-like' source (with $\Delta t \leq 0.1°$), and the expected angular size of the Coma cluster in VHE γ-rays is $\leq 0.5°$. Thus, in the case of a high CR proton content in Coma the fluxes of the π^0-decay radiation, as well as the size of the emission region, could be measured at both high and very high energies. It is important to note also that at GeV and lower energies the spectral shape of π^0-decay radiation is not sensitive to the spectral distribution of CRs at very high energies. Therefore it would be possible in principle to recover the spectral shape of γ-ray fluxes of electronic origin in the $(0.1 - 1)\,$GeV region even if VHE emission of Coma were not detected.

Acknowledgements. We would like to thank the organizers, Hans Böhringer and Luigina Feretti, for the opportunity to present these ideas at Ringberg Workshop. We would like also to thank Felix Aharonian for stimulating discussions. The work of AMA was supported through the Verbundforschung Astronomie/Astrophysik of the German BMBF under the grant No. 05-2HD66A(7).

References

[1] Aharonian F. A., Hofmann W., Konopelko A. K., Völk H. J., 1997, Astropart. Phys. 6, 343; 369.
[2] Atoyan A. M., Völk H. J., 1999, in preparation
[3] Bloom E.D., 1996, Space Sci. Rev. 75, 109.
[4] Berezinsky V. S., Blasi P., Ptuskin V. S., 1997, ApJ 487, 529.
[5] Bowyer S., Berghöfer T. W., 1998, ApJ 505, 502.
[6] Bridle A. H., Purton C. R., 1968, AJ 73, 8.
[7] Briel U. G., Henry J. P., Böhringer H., 1992, A&A 259, L31
[8] Colafrancesco S., Blasi P., 1998, Astropart. Phys. 9, 227.
[9] Deiss B. M. , 1997, A&A 325, 74
[10] Enßlin T. A., Biermann P. L., 1998, A&A 330, 90.
[11] Feretti L., Dallacasa D., Giovannini G., Tagliani A., 1995, A&A 302, 680.
[12] Fusco-Femiano R., Dal Fiume D., Feretti L., Giovannini G., Grandi P., Matt G., Molendi S., Santangelo A., 1999, ApJ 513, L21.
[13] Ginzburg V. L., 1979, *Theoretical Physics and Astrophysics*, Pergamon Press, Oxford.
[14] Giovannini G., Feretti L., Venturi T., Kim K.-T., Kronberg P. P., 1993, ApJ 406, 399.
[15] Giovannini G., Tordi M., Feretti L., 1999, New Astron. 4, 141.
[16] Hwang C.-Y., 1997, Science 278, 1917.
[17] Kim K.-T., Kronberg P. P., Dewdney P. E., Landecker T. L., 1990, ApJ 355, 29.
[18] Konopelko A. K., for HEGRA collaboration, in: J. Medina, ed. *Rayos Cosmicos 03 98: Proc. 16th European Cosmic Ray Simposium"*, to appear; *astro-ph/9901094* (1999)
[19] Kronberg P. P., 1994, Rep. Prog. Phys. 57, 325.
[20] Lieu R., Mittaz J. P. D., Bowyer S., Lockman F. J., Hwang C.-Y., Schmitt J. H. M. M., 1996, ApJ 458, L5.
[21] Lieu R., Ip W.-H., Axford W. I., Bonamente M., 1999, ApJ 510, L25.
[22] Mittaz J. P. D., Lieu R., Lockman F. J., 1997, ApJ 498, L17.
[23] Rephaeli Y., Gruber D., Blanco P., 1999, ApJ 511, L21
[24] Sarazin C., Lieu R., 1998, ApJ 494, 177.
[25] Schlickeiser R., Sievers A., Thiemann H., 1987, A&A 182,21.
[26] Sreekumar P., et al., 1996, ApJ 464, 628.
[27] Völk H. J., Aharonian F. A., Breitschwerdt D., 1996, Space Sci. Rev. 75, 279.
[28] Völk H. J., Atoyan A. M., 1999, Astropart. Phys. 11, 73.

Proceedings of the Workshop: *"Diffuse Thermal and Relativistic Plasma in Galaxy Clusters"*
Ringberg Castle, Germany, April 19–23, 1999, eds. H. Böhringer, L. Feretti & P. Schuecker, MPE Report 271, pp. 219-222

Some Aspects of Inverse Compton Emission from 3K Background Photons

Dan E. Harris[1] **and Lindsay S. Moore**[2]

[1] Smithsonian Astrophysical Observatory, 60 Garden St., Cambridge, MA 02138, USA; harris@cfa.harvard.edu
[2] Bryn Mawr College, Bryn Mawr, PA USA; lmoore@brynmawr.edu

Abstract. We review the history and a few features of IC/3K emission. We discuss observing strategies, the physical parameters which can be derived directly or indirectly from successful detections, and the disparities between magnetic field strength estimates found by different methods.

1. Introduction

The recent history of inverse Compton emission from cosmic background photons and relativistic electrons (IC/3K) began during the period when the origin of extended X-ray emission from clusters of galaxies was unclear. Felten and Morrison (1966), Blumenthal & Gould (1970), and Jones, O'Dell & Stein (1974) were among those who worked out the details of IC/3K, but not until iron lines were detected in the X-ray spectra was it generally accepted that the bulk of the X-ray emission was caused by the thermal bremsstrahlung process.

Although there were many attempts to isolate IC/3K emission from clusters, these were thwarted by the strong thermal emission which is quasi ubiquitous in clusters. The recent breakthrough came from the dual detections of IC/3K from the lobes of Fornax A: spatially with the ROSAT PSPC (Feigelson et al. 1995) and spectrally with ASCA (Kaneda et. al. 1995). In the last two years, there have been papers published on other sources which are relatively free of hot gas emission and from cluster radio halos, both from EUV excesses and from the harder spectral component at energies for which the thermal X-rays are dropping exponentially.

2. Salient Features

In this section, we list a few of the attributes of IC/3K emission which are often overlooked.

2.1. Every Non-Thermal Radio Source also Emits IC/3K Emission

IC/3K emission is mandatory: every (non-thermal) radio source in the universe is an emitter. This statement entails only the assumption that the 3K background is indeed universal. Thus the only problem is to see if it is strong enough for detection with a given system, and if it can be separated from other emissions.

2.2. Electron Energy and the Observing Frequency

At a given (X-ray) energy, we will be sampling the relativistic electron spectrum at the same value of electron energy (γ) for every source in the universe. This is because the peak frequency, ν_o, of the cosmic background spectrum (where the major contribution to the photon energy density occurs) increases as (1+z). A given electron with Lorentz energy, γ, emits most of its radiation at $\gamma^2 \times \nu_o$ and the emitted photons at that energy are redshifted by (1+z) when observed on Earth. Thus soft X-rays (1-2 keV) sample $\gamma \approx 1000$ no matter what the redshift. Attempts to integrate these electrons in order to explain a significant part of the soft X-ray background have not been successful.

2.3. The Importance of Determining the Amplitude of the Electron Spectrum at Low Energies

For B<5μG, low energy electrons (e.g. γ <1000) are not visible via their synchrotron (radio) emission because the ionosphere blocks frequencies below $\approx$ 20 MHz. Since these electrons normally have long lifetimes in the weak magnetic fields typically found in extended radio sources, they accumulate over the life of a radio source. In a sense we are sampling an encapsulated history of the radio source: the electron spectrum at low energies tells us about all the electrons produced over the source's lifetime.

3. Observing Strategies - Avoid Hot Gas!

- By going to higher energy: e.g. BeppoSax and RXTE
- By getting outside clusters: e.g. Fornax A lobes and relic radio galaxies such as 0917+75 (Harris et. al. 1995).
- Choose radio sources with large numbers of low energy electrons. This can be achieved by choosing sources

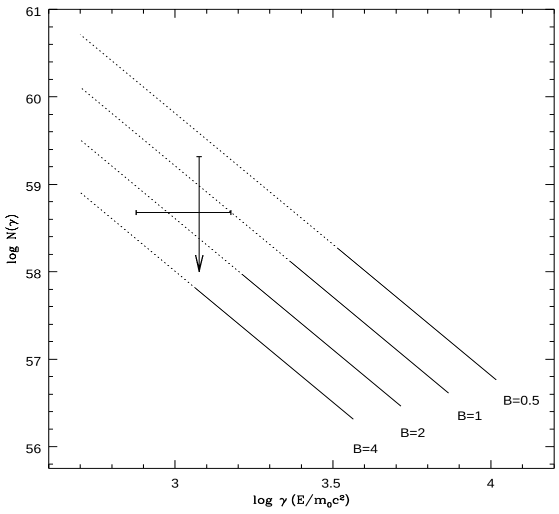

Fig. 1. Constraints on the electron spectrum for the relic radio galaxy, 0917+75 (taken from Harris et al. 1995). Heavy lines show possible segments of the electron spectrum, each labelled with a trial value of the magnetic field strength (in μG). The ROSAT derived upper limit is the only firm datum.

likely to have relatively more low energy electrons and to have weak magnetic fields since these require more electrons to get a given radio intensity. Therefore, steep spectrum, low brightness radio sources are best.

4. Rewards

Although most of us like to believe that a successful detection of IC/3K yields the average magnetic field strength directly, what we really measure is the amplitude of the electron spectrum at some low energy. To obtain the average field strength, there is still the uncertainty of the form of the electron spectrum between the direct measurement afforded by the IC/3K observation and the segment of the electron spectrum responsible for the radio emission. This is illustrated in figure 1. Since we can't be sure that a single power law extrapolates from the radio derived segment of the spectrum to the X-ray derived amplitude, the average value of B is uncertain (even if the ROSAT point were not an upper limit).

The electron spectrum below γ=1000 is of particular interest because in weak field regions (and z<0.5), E^2 halflives can approach 10^9 yr. Therefore, the total number of electrons in this energy range serves as a diagnostic of the total energy of a source during its life. While soft X-rays (e.g. 1.5 keV) provide a direct measurement of the number of electrons at γ=1000, EUVE data can provide estimates at γ=300. In Table 1 we have calculated log N (100< γ <1000) for a variety of radio sources by extrapolating their observed spectra to lower energies.

Table 1 Number of low energy electrons from extrapolated radio spectra

Source	Component	z	α_r	B(eq) (μG)	logV (cm^3)	logN	τ (yrs)
FRII							
Cyg A	2 lobes	0.057	0.6	25	69.83	63.59	1E7
RELICS							
0917	total	0.12	1.0	0.7	72.77	64.23	8E8
Coma	total		1.18	0.3	72.19	64.53	1E9
CenB	1 lobe	0.012	0.8	1.5	71.14	63.32	9E8
1358+30		0.11	0.72	0.9	72.00	63.22	8E8
1401-33		0.0136	1.44	8	71.67	64.91	1E9
3C 326	giantRG	0.089	0.82	0.8	73.46	64.75	9E8
IC2476		0.027	1.1	0.7	71.57	63.80	1E9
FRI							
3C 31		0.016	0.63	1.5	70.61	61.97	9E8
0715	1arm	0.07	1.1	4	...	62.40	...
1718	halo	0.162	1.3	6	...	62.90	...
HALOS							
Coma	total	0.023	1.34	0.5	72.64	65.28	1E9

Notes to Table 1
z is the redshift
α_r is the radio spectral index
B(eq) is the equipartition field
V is the source volume
N is the integrated number of electrons for 100< γ <1000
τ is the halflife for γ=1000 electrons.

While there are considerable uncertainties on the magnetic field and volume estimates, a substantial difference is seen for log N amongst Cyg A and relics; FRIs; and the Coma halo. These values support the notion that the relics were once FR II radio galaxies and that if cluster halos arise from the remnants of FR I galaxies such as tailed radio galaxies, it would require of order 1000 such contributions in 10^9 years.

Once an estimate of the average magnetic field strength is obtained, inferences can be made on the total energy density, $u(tot)$, and thus on the composition of the relativistic particles. There are two contributions to the particle energy density, $u(p)$, which are not 'counted' by the radio observations: low energy electrons and relativistic protons. For low brightness radio sources, it is probably the case that most of the source is 'relaxed' in the sense that there are not active shock regions (e.g. hotspots) and equipartition between magnetic field energy density, $u(B)$, and $u(p)$ is a reasonable expectation. Thus knowledge of $u(B)$ translates to an estimate of $u(p)$ and $u(tot)$. If the required $u(p)$ is large enough, the presence of relativistic protons may be indicated. The major uncertainty in this process is probably the unknown filling factor, ϕ, and if ϕ is substantially less than unity, the additional question: "Do the particles and field occupy the same volume?".

5. Discussion

5.1. *Distinction Between Radio Lobes (Including Relics) and Cluster Halos*

While we have some evidence that relativistic and thermal plasmas are spatially distinct in the case of lobes of radio galaxies (e.g. Cygnus A, Carilli et al. 1994), we do not have any confidence as to the situation for cluster halos. This is partly caused by the uncertainty concerning the genesis of radio halos in clusters. If relativistic plasma is completely mixed with the thermal plasma, then it is reasonable to assign a value close to unity for the filling factor, ϕ, but if the actual synchrotron emitting regions are to be distinct from the thermal plasma (in the sense of a magnetic boundary separating the two), then ϕ is most likely quite small. In the former case we should probably include the thermal energy density in any application of the equipartition condition, whereas in the latter case, we would be justified in balancing the relativistic particle energy density with the magnetic field energy density.

In a sense, we have two distinct problems. For relics and radio lobes such as Fornax A, we do not have to contend with excessive thermal emission and can get a fairly clean measurement if IC/3K intensity and distribution. But for clusters, it is only with difficulty that we avoid the thermal contamination.

What are the implications of the fact that some estimates of the Coma field strength are in reasonable accord with the minimum energy B field for ϕ=1 and $u(p)$=$u(B)$? If the synchrotron emitting plasma were distinct from the cluster gas and ϕ <<1, then the equipartition field B(eq) would be much larger than the IC/3K estimate, and that does not seem to be the case.

5.2. Current IC/3K Detections and the Implied B Fields

Using the relationships of Harris & Grindlay (1979), we have calculated the value of the average magnetic field strengths in some of the sources for which IC/3K detections have been claimed or an upper limit has been measured. These are presented in Table 2 together with magnetic field estimates published by the authors.

5.3. Comparison of B Field Estimates

The B field estimates for clusters discussed at this workshop can be roughly divided into 3 categories, depending on the method used and the type of source.

B=0.1 to 0.2 μG

These sorts of values were put forward on the basis of the excess X-ray flux observed over that expected from the hot gas in the Coma cluster. Both the EUV excess and the BeppoSax measurements yield B values <0.2 μG. Fusco-Femiano et al. (1999) give fx(20-80keV)=2.2×10^{-11} ergs cm^{-2} s^{-1} and B≈ 0.15 μG. Note however that Henriksen (1998) using ASCA and HEAO-I data obtained an upper limit of fx(20-60keV)<2.9×10^{-12} ergs cm^{-2} s^{-1} and B>0.26 μG.

B≈ few μG

Magnetic field strengths of a few μG have been derived from equipartition calculations for the Coma radio halo, from the IC/3K estimates for the lobes of Fornax A, and from some estimates for clusters from Faraday rotation.

B = 5 to 20 μG

These stronger B field estimates generally come from the Faraday rotation measurements of unresolved sources in or behind clusters. The greatest uncertainty here is the scale size of magnetic field cells (for which the fields can reverse direction). If there are a large number of cells along the line of sight which have sufficient field strength and electron density to make a substantial contribution to the Faraday rotation, then the required B field will be significantly larger than for the case of only a few cells.

While we are not in a position to resolve the disparity in these B field estimates, we suspect that typical field strengths in clusters and relaxed radio lobes probably lie within the range 0.5< B <3μG. If this were to be the case, then published EUV and hard X-ray excesses are either wrong or arise from an emission process other than IC/3K and clusters have large scale coherent fields so that there are relatively few field reversals along the line of sight.

6. Conclusion

We have a fairly good idea of the problems involved in using IC/3K emission to derive physical quantities. Most of these difficulties are not going to go away soon, but the quality of the X-ray data should improve significantly with the advent of several missions with larger collecting area, better resolution, and extended frequency coverage.

References

[1] Bagchi, J., Pislar, V., and Lima Neto, G.B. 1998 MNRAS 296, L23
[2] Blumenthal, G.R. and Gould, R.J. 1970 Rev. Mod. Phys. 42, 237
[3] Carilli, C.L., Perley, R.A., and Harris, D.E. 1994 MNRAS 270, 173
[4] Feigelson, E.D., Laurent-Muehleisen, S.A., Kollgaard, R.I. Fomalont, E.B. 1995 ApJ 449, L149
[5] Felten, J.E. and Morrison, P. 1966 ApJ 146, 686
[6] Fusco-Femiano, R., Dal Fiume, D., Feretti, L., Giovannini, G., Grandi, P., Matt, G., Molendi, S., and Santangelo, A. 1999 ApJ 513, L21
[7] Harris, D.E. and Gindlay, J.E. 1979 MNRAS 188, 25
[8] Harris, D. E., Willis, A.G., Dewdney, P.E., and Batty, J. 1995 MNRAS 273, 785
[9] Henriksen, M. 1998 PASJ 50, 389
[10] Jones, T.W., O'Dell, S.L., and Stein, W.A. 1974 ApJ 188, 353
[11] Kaneda, H. Tashiro, M., Ikebe, Y., Ishisaki, Y., Kubo, H., Makshima, K., Ohashi, T., Saito, Y., Tabara, H, and Takahashi, T. 1995 ApJ 453, L13
[12] McAdam, W. B. 1991 Proc. ASA 9 (2) 255
[13] Tashiro, M., Kaneda, H, Makishima, K., Iyomoto, N., Idesawa, E., Ishisaki, Y., Kotani, T., Takahashi, T., and Yamashita, A. 1998 ApJ 499, 713

Table 2 Magnetic field estimates from IC/3K detections

		Luminosities			B Fields(A)		B Fields(RX)	
		Log Lr	Log Lx	Lr/Lx	B(eq)	B(ic)	B(eq)	B(ic)
		(erg/s)			(μG)		(μG)	
CLUSTERS								
Coma 1		40.85	43.71	0.001	...	0.15	0.2	0.05
RADIO LOBES								
Fornax A								
	Keast	41.40	40.95	3.24	...	2.4	1.0	1.8
	Kwest	41.64	40.89	5.62	...	3.5	1.0	2.6
	Fwest	41.78	41.08	5.01	3.0	1.9	1.4	2.0
RELICS								
A 85	0038-096	41.80	42.95	0.07	...	0.9	2.2	0.4
Cen B	<lobe>	42.20	41.50	5.01	...	3.1	1.4	1.7
0917	total	41.83	<42.30	>0.34	0.7	>0.7	0.7	>0.7

Notes to Table 2

Luminosities are indicative; the radio band was generally 10^7 to 10^{10} Hz (except as noted below). The X-ray bands depend on the telescopes used. B(eq) is the equipartition field (filling factor of unity and no protons) and B(ic) is the field strength derived from the IC/3K measurements. Both the original authors' values (A) and those calculated from the equations in Harris and Grindlay (1979) ['RX'] are given.

COMA 1

Entries are based on the composite radio spectrum presented by Fusco-Femiano et al. (1999); 'FF' hereafter. The general properties of the radio spectrum of the halo were checked against earlier presentations. Note however that whereas earlier work found α_r around 1.2 to 1.3, FF argue for curvature above 100 MHz, thus deducing a spectral break with an injection spectrum characterized by α=0.96. For RX inputs, we take the synchrotron band to be 30-630MHz, with a fiducial flux density of S(100MHz)=10 Jy (from their figure). The X-ray data are from BeppoSax (ibid.). FF combine two detector results and make a spectral fit with two components (thermal and a power law). For the power law, they get α_x =0.6±0.4. For the volume, we take the diameter used by FF: 25' (1 Mpc).

Fornax A

We used two papers: Kaneda et al. (1995) - ASCA spectral analysis ("Keast" and "Kwest"), and Feigelson et al. (1995)- spatial analysis from the ROSAT PSPC. Feigelson only did the West lobe ("Fwest").

A85

The results are based on Bagchi et al. (1998) from a wavelet analysis of ROSAT PSPC data.

CENTAURUS B (a.k.a. PKS1343-601)

This is a relic radio galaxy, somewhat obscured by the Milky Way. Radio data are from McAdam (1991) and the X-ray data are from Tashiro et al. (1998). Since the X-ray data are for the entire source, and since the lobes are not the same size and brightness, we model an 'average lobe', taking the size, r=300" (that of the S lobe), and divide both radio and X-ray fluxes by 2.